Synthesis and molecular assembly of benzenoid ring-mounted U-shaped septuple-bridged [7,7]orthocyclophanes walled by cofacial quinoxaline rings

ARTICLE *in* TETRAHEDRON · AUGUST 2015

Impact Factor: 2.64 · DOI: 10.1016/j.tet.2015.06.046

2 AUTHORS, INCLUDING:

Teh-Chang Chou

National Chung Cheng University

23 PUBLICATIONS **99** CITATIONS

SEE PROFILE

Tetrahedron 71 (2015) 5620–5633

Contents lists available at ScienceDirect

Tetrahedron

journal homepage: www.elsevier.com/locate/tet

Synthesis and molecular assembly of benzenoid ring-mounted U-shaped septuple-bridged [7,7]orthocyclophanes walled by cofacial quinoxaline rings

Teh-Chang Chou *, Yong-Jie Li

Department of Chemistry and Biochemistry, National Chung Cheng University, Minsyong, Chiayi 621, Taiwan

ARTICLE INFO

Article history:
Received 18 April 2015
Received in revised form 9 June 2015
Accepted 11 June 2015
Available online 18 June 2015

Keywords:
Self-assembly
π–π Stacking interaction
Orthocyclophanes
Molecular clefts
Quinoxaline

ABSTRACT

The U-shaped septuple-bridged [7,7]orthocyclophanes (**10Aa**–**c** and **10Ca**–**c**), side-walled with cofacial quinoxaline (QX) and benzoquinoxalinedione (BQXO) rings and mounted with *N*-(anthracen-9-ylmethyl)-, *N*-(naphthalen-2-ylmethyl)-, and *N*-(pyren-1-ylmethyl)succinimide ring, were, respectively, synthesized from the corresponding *N*-(4-methoxybenzyl)succinimide ring-incorporated, QX and benzoquinoxaline (BQX) ring-walled analogues molecular systems (**1A** and **1B**). The synthesis involved oxidative removal of *N*-(4-methoxybenzyl) group from **1A** and **1B** with ceric ammonium nitrate (CAN), followed by Gabriel-type N-alkylation with a proper arylmethyl bromide. The BQX ring in **1B** was found to be oxidized to BQXO ring in the CAN-oxidation step. The molecular cleft-like [7,7]orthocyclophanes thus synthesized display a tendency of self-assembly chiefly driven by intermolecular π–π stacking interaction, forming V-shaped or linear tail-to-tail (wall-to-wall) dimers that further assemble in head-to-head (aryl-to-aryl) arrangement to form tetramers and polymers. The event of molecular assembly was investigated by concentration-variant ^{1}H NMR spectroscopic and X-ray crystallographic analyses.

1. Introduction

Molecular self-assembly and recognition driven by π–π stacking, C–H/π, and other non-covalent interactions are ubiquitous and play important roles in manipulating the processes of forming highly organized structure systems (supermolecules) of biological and physiochemical significance.[1–12] Assorted phenomena and various prospective applications to medicinal, catalysis, and material chemistry have been disclosed and inspired much synthetic endeavor directed toward the molecular systems of specially designed architecture that may be used for studies of molecular self-assembly and host–guest recognition.[13–32] In this context, a class of molecular systems, the so-called molecular tweezers, clips, and clefts, have demonstrated the capabilities of self-assembly and host–guest recognition in homogeneous solution and condensed phase.[18,19] This class of molecular systems frequently utilizes a rigid or semi-rigid and often symmetrically arched polycyclic skeleton to control structural shape having concave–convex topology and to serve as 'platforms' or 'spacers' for the attachment of aromatic rings in a *syn* conformation. Notable examples are molecular clefts adopting the cyclic skeleton of Kagan's ether,[22,23] Tröger's base,[24] and bile acid,[25,26] molecular tweezers and clips designed based on polymethylene-bridged polyarene by Klärner,[27–29] and molecular clips derived from diaryl glycoluril pioneered by Rebek and Nolte.[30–32]

Recently, we developed an efficient three-step synthetic approach to the quinoxaline-based multi-bridged [*n*,*n*′] orthocyclophanes,[33–35] such as the *N*-benzylsuccinimide ring-incorporated U-shaped septuple-bridged [7,7]orthocyclophanes **1** with the generic structure **A** shown in Fig. 1.[34] The process consists of three fundamental operations: (1) the Diels–Alder reaction of 1,2,3,4-tetrachloro-5,5-dimethoxycyclopentadiene (TDCp, **2**)[36] with a suitable bis-dienophile such as **3**,[37] to construct a bis-adduct as the central spacer scaffold, (2) the conversion of dichloroetheno-bridges in the bis-adduct by ruthenium-promoted oxidation using Khan's protocol[38] to generate a bis-α-diketone, followed by (3) the construction of sidewalls (phane parts) by the condensation of the bis-α-diketone with an arene-1,2-diamine (ADA, **4**) to produce **1** (**A**) embedding face-to-face aligned quinoxaline (QX), benzoquinoxaline (BQX), dimethylquinoxaline (diMQX) or other substituted-QX rings.[33–35,39,40]

X-ray crystallographic analysis revealed that the pair of QX sidewalls in orthocyclophanes **1** (**A**) are stretching out from the rigid spacer scaffold in almost parallel (*syn*-periplanar) manner, separated

* Corresponding author. Fax: +886 5 272 1040; e-mail address: chetcc@ccu.edu.tw (T.-C. Chou).

http://dx.doi.org/10.1016/j.tet.2015.06.046
0040-4020/

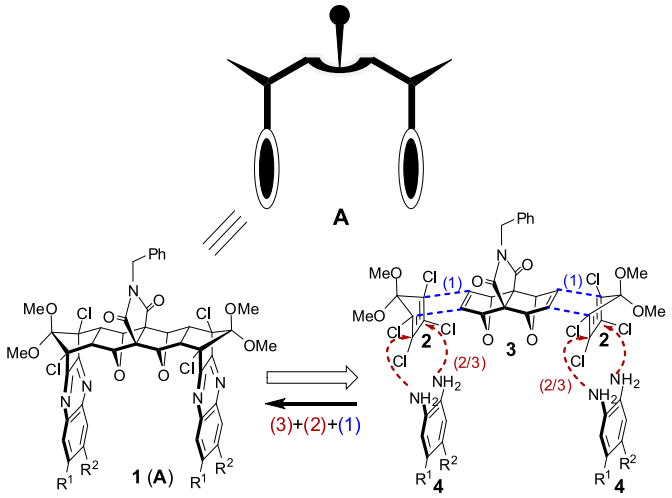

Fig. 1. An outline of retrosynthesis of septuple-bridged [7,7]orthocyclophanes **A** (**1**): (1) the construction of the spacer scaffold by Diels–Alder reaction, (2) the generation of bis-α-diketone by ruthenium-promoted oxidation, (3) the construction of quinoxaline (QX) sidewalls by the condensation.

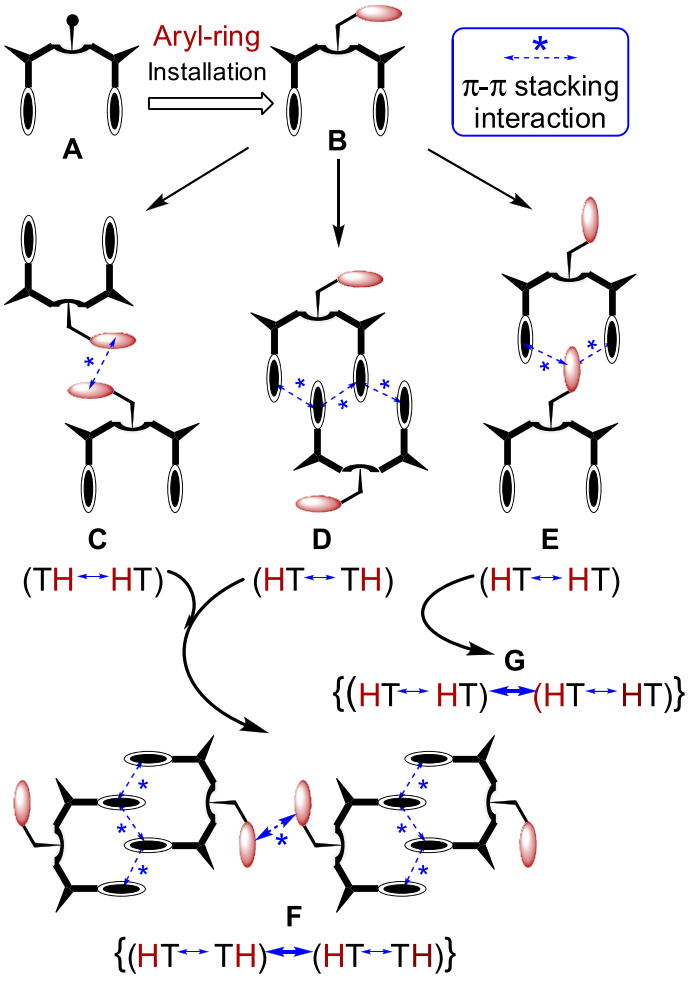

Fig. 2. Schematic representations of three possible ways of self-assembly driven by intermolecular π–π stacking interaction for the U-shaped orthocyclophanes **B** to form dimeric entities **C**, **D**, and **E** via the head-to-head (TH↔HT), tail-to-tail (HT↔TH), and tail-to-head (HT↔HT) modes, respectively. Packing by combinative modes of TH↔HT and HT↔TH leads to {(HT↔TH)↔(HT↔TH)} polymer **F**. Continuous packing by HT↔HT mode leads to {(HT↔HT)↔(HT↔HT)} polymer **G**.

by centroid-to-centroid distances of about 7.5–8.5 Å.[33,34] These distances are too distant to exhibit excimer or exciplex emission via the intramolecular π–π interaction. Such a photophysical phenomenon was displayed by the U-shaped quadruple-bridged [5,5] orthocyclophanes, wherein the aromatic sidewalls are separated by about 4.0–4.5 Å.[33,39,40] On the other hand, orthocyclophanes **1** (**A**) could belong to a family of molecules termed molecular clefts[18,19] due to their concave–convex topography with rim-to-rim distances of 7.5–8.5 Å that are suitable to form complexes with molecular substrates by clipping the substrate via π–π stacking interactions.[34,39] In all crystal structures of orthocyclophanes **1**, V-shaped dimeric entities resulting from reciprocal clipping of the aromatic sidewalls of two molecules of **1** into the opposing U-shaped cleft by angles ranging from 45 to 85° were observed.[34]

To continue our study on the self-assembly of [7,7]orthocyclophanes **1** (**A**), we were prompted to undertake the task of mounting benzenoid ring on the top (succinimide) side of **1** as **A**→**B** illustrated in Fig. 2. Since benzenoid rings such as anthracenyl and pyrenyl are apt to exert intermolecular π–π stacking interactions forming dimeric structures,[11,15] we expected that **B**, being 'bidentate' structured, could conceivably assemble to form dimers in three modes via the head-to-head (TH↔HT), tail-to-tail (HT↔TH), and tail-to-head (HT↔HT) associations, as depicted, respectively, by **B**→**C**, **B**→**D**, and **B**→**E** in Fig. 2. Subsequent assembly of dimers could lead to the formation of tetrameric **F** {(HT↔TH)↔(HT↔TH)} by head-to-head manner and **G** {(HT↔HT)↔(HT↔HT)} by tail-to-tail mode, and ultimately their respective polymers. In this paper, we describe the synthesis of benzenoid ring-mounted septuple-bridged [7,7]orthocyclophanes (**B**) and the observation of molecular self-assembly driven by π–π stacking, C–H/π, and other noncovalent interactions that direct **B** to form dimers (**C**, **D**), tetramers (**F**), and polymers in the solid state.

2. Results and discussion

2.1. Synthesis

At the onset, installation of benzenoid ring onto [7,7]orthocyclophane backbone took advantage of the known *N*-(4-methoxybenzyl)succinimide ring-fused *syn*-bis-adduct **5**[34] and employed dealkylation/alkylation via succinimide **6** as key transformation. Thus, as shown in Scheme 1, the *p*-methoxybenzy group in *syn*-bis-adduct **5**, made available from the Diels–Alder reaction of TDCp (**2**)[36] and bis-dienophile **3**,[37] was removed by oxidative cleavage with ceric ammonium nitrate (CAN)[41,42] in MeCN/H_2O (5:1) at refluxing temperature to give succinimide **6** in 80% yield. When a solution of succinimide **6** in acetone in the presence of K_2CO_3 was treated with an alkylating agent **7** [2-(bromomethyl)naphthalene (**7a**), 9-(bromomethyl)anthracene (**7b**), or 1-(bromomethyl)pyrene (**7c**)], the corresponding *N*-(arylmethyl) succinimide **8** [**8a**, **8b**, or **8c**] was obtained in excellent yield (91–93%).

Polycyclic aromatic hydrocarbons are apt to oxidation, implying that the *N*-(arylmethyl)succinimide substructure in **8** may cause complication in the subsequent conversion of the dichloroetheno-bridge into the α-diketonic moiety by RuO_4-oxidation. Accordingly, we soon abandoned this synthetic route and adopted the approach that postponed the oxidative removal of the *p*-methoxybenzyl group until the installation of QX sidewalls had been accomplished; that is, to prepare the known QX-walled [7,7]orthocyclophanes **1A** and **1B** in advance (Scheme 1).[34]

Thus, as shown in Scheme 1, when employing $RuCl_3 \cdot xH_2O$ (0.44 equiv) and $NaIO_4$ as oxidant (2.5 equiv) and stirring in a solvent system of $CHCl_3$/MeCN/H_2O (3:3:1) at 0 °C for 24 h, RuO_4-oxidation of

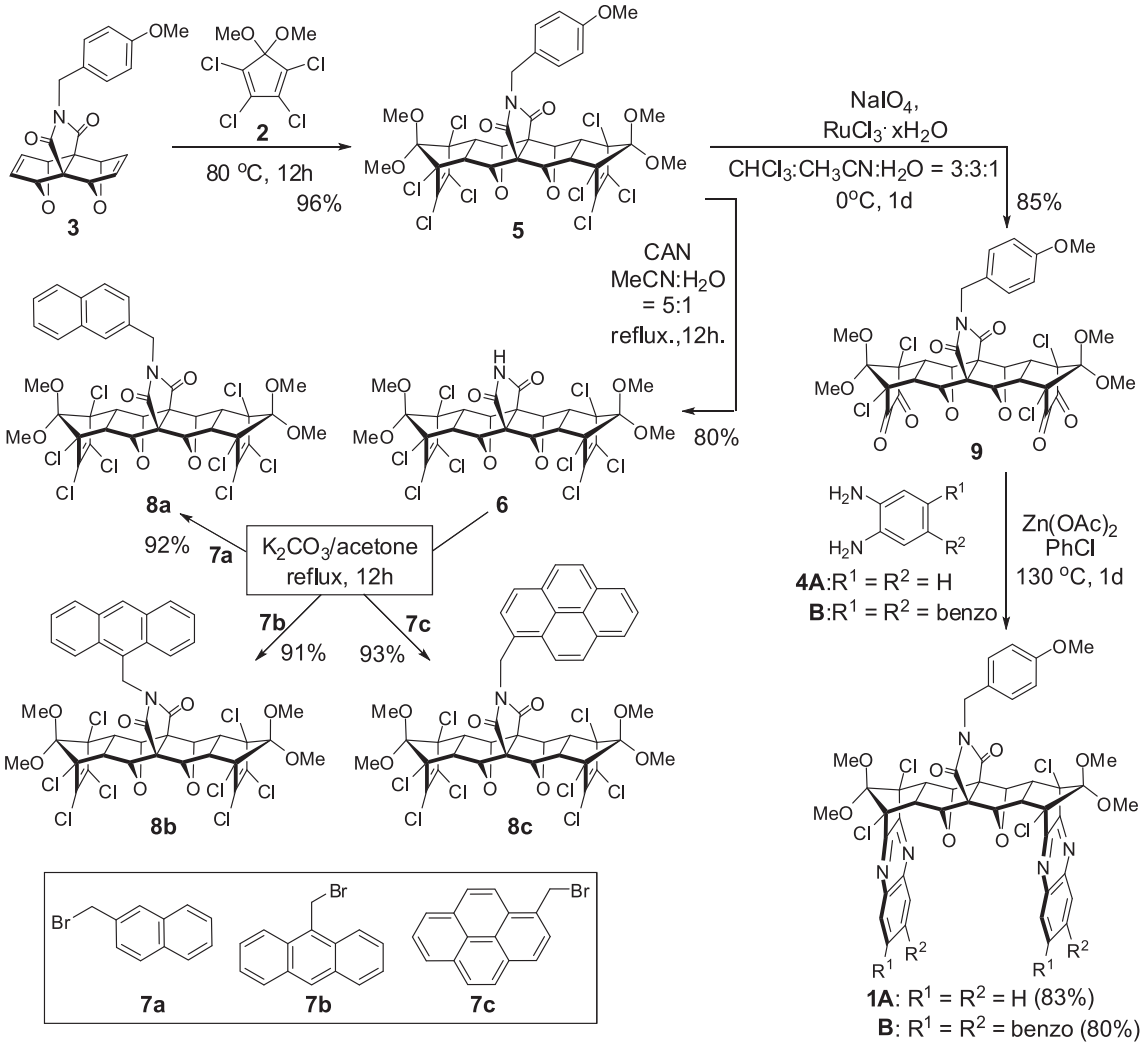

Scheme 1.

syn-bis-adduct **5** smoothly provided yellow bis-α-diketone **9** in 85% yield. The condensation of bis-α-diketone **9** with benzene-1,2-diamine (**4A**) or naphthalene-2,3-diamine (**4B**) was executed by performing the reaction in PhCl at 130 °C for 24 h in the presence of $Zn(OAc)_2$ as a catalyst. The resultant *N*-(4-methoxybenzyl)succinimide ring-fused QX-walled [7,7]orthocyclophanes **1A** and **1B** were obtained in yields of 83% and 80%, respectively.[34]

As shown in Scheme 2, removal of *p*-methoxybenzyl group from QX-walled **1A** by the CAN-oxidation in $MeCN/H_2O$ (5:1) at room temperature afforded the succinimide ring-fused, QX-walled [7,7] orthocyclophane **10A** in 68% yield. However, when benzoquinoxaline (BQX) walled **1B** was subjected to the CAN-oxidation in the same solvent system at refluxing temperature for 24 h, its *p*-methoxybenzyl group was removed, accompanied by the oxidation of BQX walls, furnishing the succinimide ring-fused, benzoquinoxalinedione (BQXO) ring-walled **10C** in 59% yield. No expected BQX-walled **10B** was found.

As shown in Scheme 3, treatment of **10A** and **10C** in acetone with an alkylating agent **7a**, **7b** or **7c** in the presence of K_2CO_3 achieved Gabriel-type N-alkylation and delivered the corresponding *N*-(arylmethyl)succinimide ring-fused [7,7]orthocyclophanes bilaterally walled with QX rings (**10Aa**, **10Ab**, and **10Ac**) and BQXO rings (**10Ca**, **10Cb**, and **10Cc**), respectively, in excellent yields (92–96%).

2.2. X-ray crystallographic study

Single crystals of septuple-bridged [7,7]orthocyclophanes **10A**, **10Ac**, **10Ca**, and **10Cc** suitable for room-temperature X-ray structural determination were obtained by recrystallization. The ORTEP drawings of X-ray crystal structures are depicted in Fig. 3 and the tables for crystal data/structure refinement are compiled in Tables S1–S4 in Supplementary data.

Tables 1 and 2 list some selected parameters from the X-ray crystal structures of **10A**, **10Ac**, **10Ca**, and **10Cc**, which describe the molecular structures and packing motifs within and among dimeric entities. Two conformations with different mean interplanar distance and angle were noted for the crystal structure of **10Ac**, probably due to steric constrain resulting from reciprocal clipping to form the V-shaped dimeric entity in the crystal packing. Three compounds (**10A**, **10Ca**, and **10Cc**) co-crystallized with solvent and the selected close contacts ($d_{H\cdots X}$, X=C, O, or N) that involve solvate molecules in the crystals are listed in Table S5 in Supplementary data.

In general, the geometrical features of these new aryl ring-appended QX-walled [7,7]orthocyclophanes are similar to **1** (**A**, Fig. 1) reported previously.[34] As shown in Fig. 3 (face view) and Table 1, the pair of face-to-face QX rings in **10A**, **10Ac**, **10Ca**, and **10Cc** is suspended from the rigid spacer scaffold in almost parallel

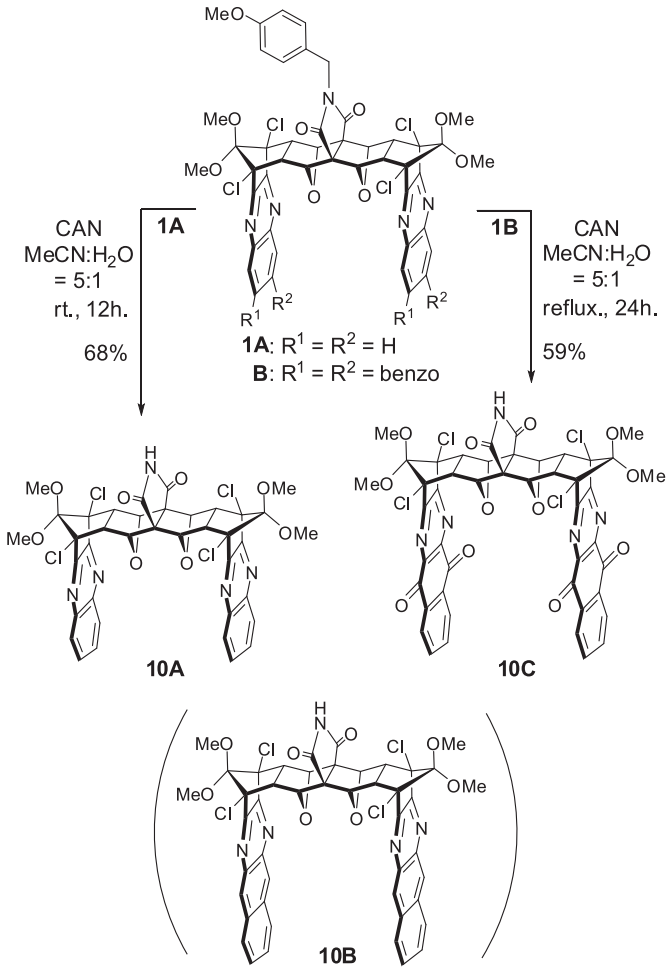

Scheme 2.

manner indicated by small QX–QX mean plane angles (∠°). The QX rings in **10A** stretch out in a slightly outward (average $d_{N-N}<d_{C-C}$, diverging) manner and those in **10Ac**, **10Ca**, and **10Cc** in an inward (average $d_{N-N}>d_{C-C}$, converging) style. Similar to the appended phenyl ring in **1**,[34] the appended benzenoid ring in **10Ac**, **10Ca**, and **10Cc** is inclined alongside, rather than vertically, to the molecular framework (side view, Fig. 3) in the rotation-constrained solid state. This pattern of alignment probably benefits from the intramolecular CH–π interactions of aryl ring with the polarized C–H bonds of methoxy group,[8,34,43–46] indicated by short OCH_3···Ar–centroid distance (Table 1).

The distances between the centroids of the face-to-face QX rings in the crystal structures of **10A**, **10Ac**, **10Ca**, and **10Cc** are 8.465, 7.521 (7.562), 7.370 Å, and 7.384 Å, respectively, and are dependent on the mean plane angles of these aromatic rings (Table 1). This range of intercentroid distances is suitable for clipping to form dimeric entity motivated by π–π stacking interactions.[2,34,47–50] Accordingly, all molecules of **10A**, **10Ac**, **10Ca**, and **10Cc** display self-assembly leading to the formation of tail-to-tail (HT↔TH, **D**, Fig. 2) dimeric entities in their crystal structures (Figs. 4 and 5).

Resembling orthocyclophanes **1**,[34] the QX sidewalls of two molecules of **10A** and **10Ac** clip reciprocally into the opposing U-shaped cleft to form V-shaped self-assembly dimeric entities with molecular clipping angles of 43° and 55°, as illustrated in Fig. 4a and b, respectively. The distinctive features of dimeric structures differently displayed by **10A** and **10Ac** are the mean plane angle (∠°) and intercentroid distance ($d_{\bullet\cdots\bullet}$) between adjacent QX rings (Table 1). In **10A** dimer (Fig. 4a), the QX rings are tilted with respect to one another by angles (∠°) of 11.27°/21.56°/11.27° and separated by distances ($d_{\bullet\cdots\bullet}$) of 5.564 Å/5.859 Å/5.564 Å, indicating that these QX rings probably benefit from C–H/π interactions ($d_{C\cdots H}$=3.361 Å/4.555 Å/3.361 Å, Table 1).[51–53] On the other hand, the QX rings in **10Ac** dimer evidently benefit from direct π–π stacking interactions in a parallel-displaced orientation[47–50] because of near coplanarity of QX rings (Fig. 4b), as suggested by smaller angles (∠°=8.56°/3.09°/5.43°) and shorter distances ($d_{\bullet\cdots\bullet}$=4.685 Å/4.598 Å/4.515 Å, $d_{C\cdots C}$=3.524/3.840/3.566, Table 1).

Further examination of the packing of the dimeric structures of **10A** and **10Ac** reveals that they are held together by a second type of intradimeric interactions taking advantage of inherent oxa-bridge (H–C–O–C–H) by making use of H-bonds (Table 1).[54–56] As shown in Fig. 4, pairwise close contacts between polarized C–H bonds of oxa-bridges of one molecule and heteroatoms (bridgehead chlorine and nitrogen of internal QX rings) of adjacent molecule are observed in the dimeric structures of **10A** and **10Ac** (Table 1). In addition, the internal QX rings are located close to the oxygen atoms at oxa-bridges of partner molecule to exert QX–H···O hydrogen bonding interactions. In the dimeric structure of **10A** (Fig. 4a), close contacts by the mode of C=O···Cl (3.070 Å) are observed.[57,58]

Interestingly, the benzoquinoxalinedione (BQXO) ring-walled [7,7]orthocyclophane **10Ca** and **10Cc** exhibit self-assembly to form dimeric entities in a distinctive way. As illustrated in Fig. 5, the BQXO sidewalls of two molecules of **10Ca** and **10Cc** clip reciprocally into the opposing U-shaped cleft in an antiparallel manner (clipping angle: 180°), forming a linear HT↔TH dimeric structure. These are the first cases of self-assembly leading to tail-to-tail dimeric structure of linear geometry for the U-shaped septuple-bridged [7,7]orthocyclophanes **A** (Fig. 1).

Evidently, dimerization of **10Ca** and **10Cc** is driven by direct π–π stacking interactions between face-to-face aligned BQXO rings.[47–50] The two *internal* rings are coplanar (∠°=0.00°) and separated by a distance of 3.656 Å ($d_{\bullet\cdots\bullet}$=4.724 Å) and 3.615 Å ($d_{\bullet\cdots\bullet}$=4.634 Å), respectively (Table 1). The remaining pairs (e.g., external/internal) of BQXO rings are only slightly tilted with respect to one another (∠°=5.83° and 5.52°) and separated by a shorter distance of 3.405 Å ($d_{\bullet\cdots\bullet}$=4.611 Å) and 3.433 Å ($d_{\bullet\cdots\bullet}$=4.639 Å), respectively. The dimeric structures are further sustained by QX–H···O–CH close contacts.[55] As shown in Fig. 5a, within the **10Ca** dimeric packing motif, internal BQXO rings are nearly symmetrically disposed against the oxa-bridges of associated molecule to exhibit two pairs of binary QX–H···O–CH close contacts with distances of 2.76–2.91 Å. In the case of **10Cc** dimer (Fig. 5b), the corresponding binary close contacts are equivalent with distances of 2.587 Å and 2.591 Å, indicating exactly symmetrical disposition of their internal BQXO rings against the oxa-bridges (Table 1). In addition, as shown in Fig. 5 and Table S5, the packing motifs for **10Ca** and **10Cc** appear to be secured by solvate molecules (CH_3CN), which fasten two monomers via interactions of CN···HC–O (2.378 Å), CN···H–QX (2.654 Å), and $NCCH_3$···O=C (2.515, 2.680 Å).

Why do compound **10Ca** and **10Cc** form tail-to-tail dimeric entities by linear arrangement whereas others (**10A**, **10Ac**, and **1**'s) adopt V-shaped geometry? On the basis of an examination of the kind of QX-walls and the structure of the dimeric **10Ca** and **10Cc**, we suggest that the presence of additional electron-accepting benzoquinone ring in the sidewalls play an important role in packing preferences. As shown in Fig. 5 (side-view), the π-stacked BQXO-walls are shifted along the molecular axes such that the π-deficient benzoquinone ring is packed face-to-face against relatively electron-rich terminal benzene ring.[8,59] Such an arrangement could fortify direct π–π stacking interactions, which surpass the need of interatomic non-covalent interactions to drive self-assembly, such as H-bonds (CH···X) found in the V-shaped dimeric structure.

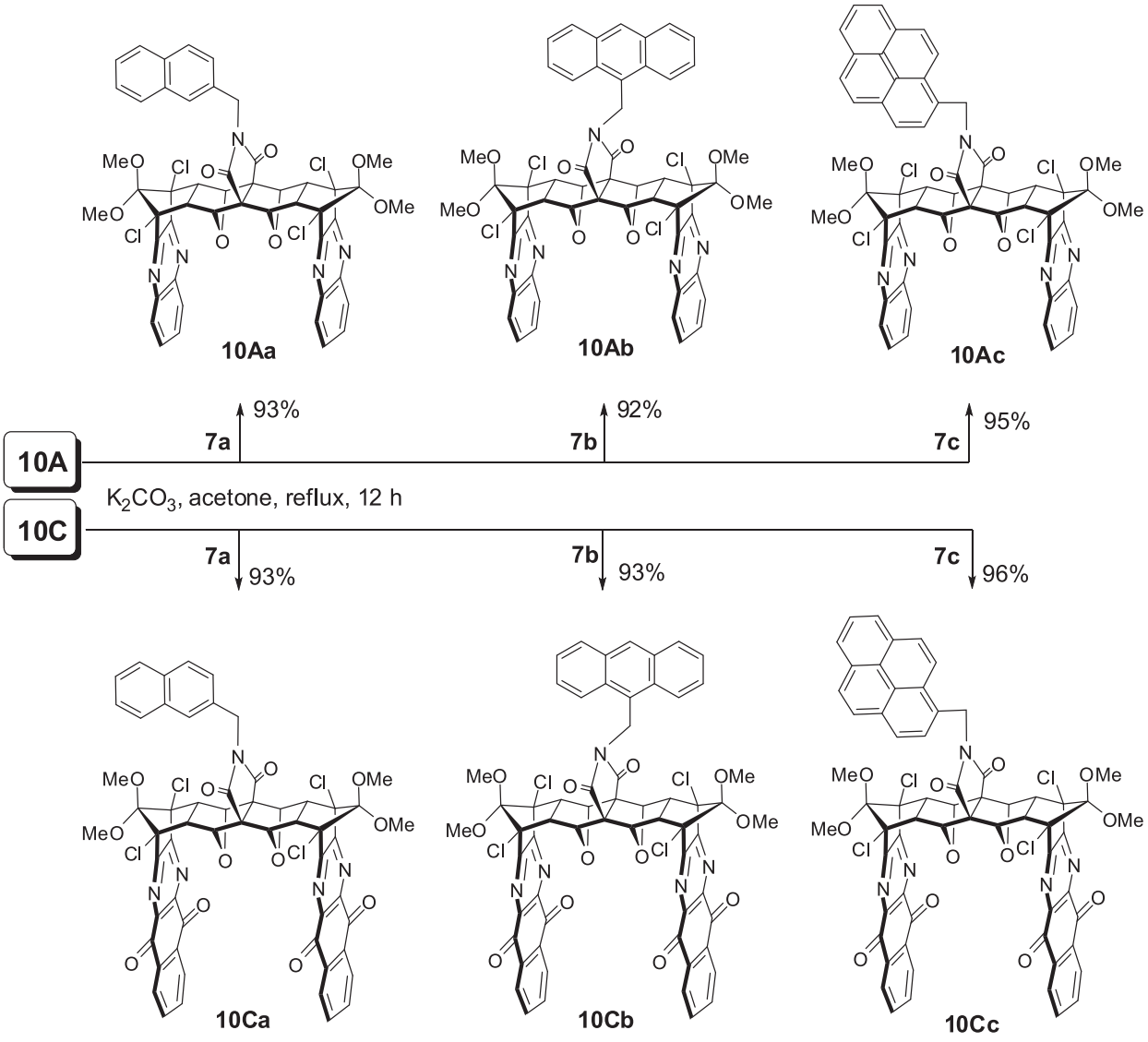

Scheme 3.

We next examine how the tail-to-tail (HT↔TH) dimers employ their 'heads'—the appended aryl rings—to unite and form the {(HT↔TH)↔(HT↔TH)} tetrameric entities and their subsequent packing into polymers to construct two-dimensional structure in the crystals. Compound **10A** co-crystallized with ethyl acetate (AcOEt). As shown in Fig. 4a, each molecule of **10A** in the V-shaped dimer grasps a solvate molecule on its bridgehead hydrogen of oxa-bridge via O···H–C–O close contact (2.617 Å) with the ethoxy oxygen of AcOEt. This AcOEt molecule is then connected to the hydrogen at succinimide ring of a nearby molecule of **10A** via N–H···O=C hydrogen-bonding interaction (1.979 Å/170.78°) as depicted in Fig. 6a. Interestingly, AcOEt molecules assume a conformation to allow the oxygen atoms of succinimide ring and oxa-bridge in **10A** to execute OCH_2···O close contacts with the polarized OCH_2 group (2.932 Å and 2.790 Å, respectively). A molecular array thereby structured by molecules of EtOAc-attached **10A** in a tail-to-head mode (HT↔HT↔HT, **G**, Fig. 2) is allied to adjacent analogous molecular array by clipping manner leading to the formation of two-dimensional network of crystal of **10A** (Fig. S1 in Supplementary data).

The V-shaped dimeric **10Ac** forms rhombus-like structured tetramers $\{(HT\leftrightarrow TH)^2\}$ in the crystal. As depicted in Fig. 6b, tetramerization is manifestly driven by π–π stacking interactions between face-to-face aligned pyrenyl rings; the aromatic rings are almost coplanar (∠°=0.5°) with a centroid-to-centroid distance of 3.914 Å and a shortest interplanar carbon-to-carbon distance of 3.412 Å. This offset π–π stacking motif also gains assistance from dispersive interactions between CH_2 groups and the adjacent Ar ring, suggested by short N–CH_2···C_{Ar} distances of 2.856 Å and 2.959 Å (Table 2). The resulting rhombus-like structured tetramers form molecular sheets on *bc*-plane (Fig. S2 in Supplementary data) via side-by-side reciprocal ArH···O=CN (2.446 Å/2.779 Å) and ArH···Cl (3.041 Å/3.317 Å) interactions,[54] which subsequently pack against one another along the crystallographic *a*-axis to form three-dimensional structure of crystalline **11Ac** employing OCH_3···Ar interactions (hydrogen-to-centroid distance: 2.654 Å/2.673 Å) and OCH_3···OCH_3 close contacts (2.566 Å, Table 2).[43–46,54]

Fig. 7 illustrates the arene–arene (π–π stacking and C–H/π) interactions that control the subsequent packing of two linear tail-to-tail (HT↔TH) dimeric entities (**10Ca** and **10Cc**) to form head-to-head {(HT↔TH)↔(HT↔TH)} tetramer and ultimately linear polymers in the crystal (**F**, Fig. 2). Unlike pyrenyl rings, which are apt to stack co-facially via π–π stacking interaction, naphthalenyl rings commonly prefer to adopt T-shaped geometry to exert C–H/π

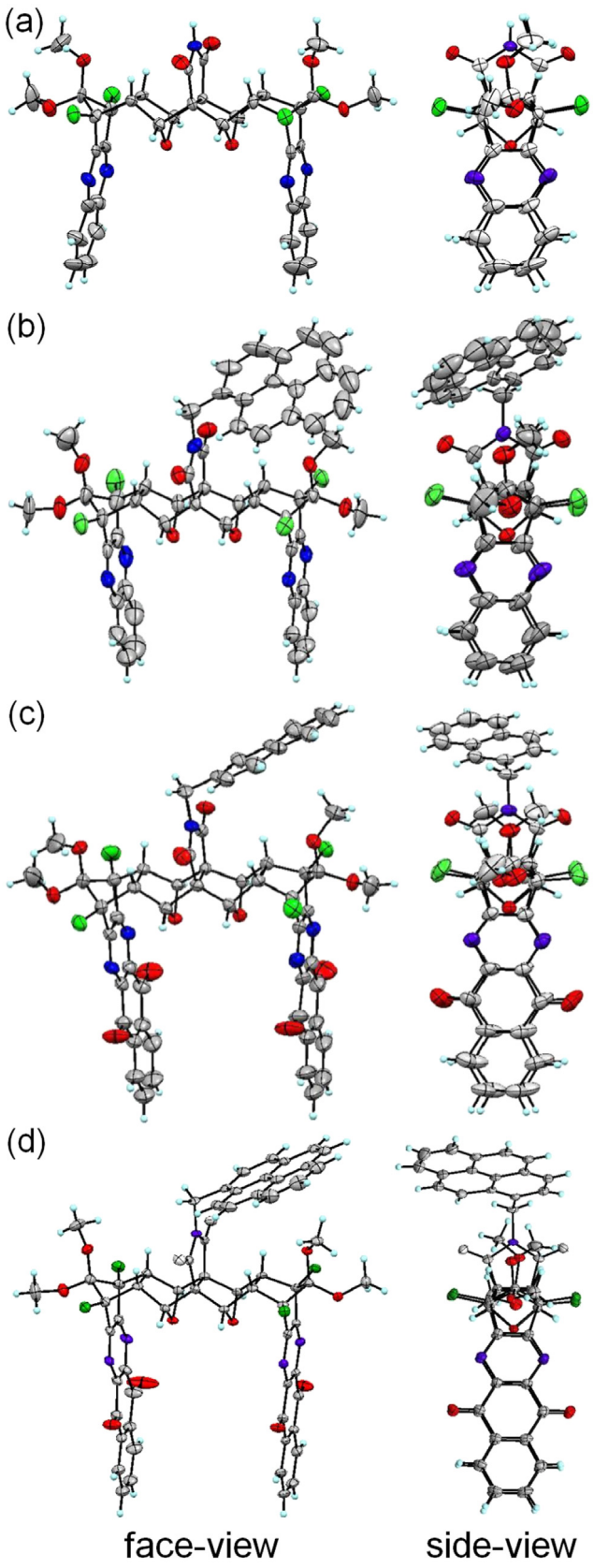

Fig. 3. The ORTEP drawings of the molecular structures of [7,7]orthocyclophanes: (a) **10A**, (b) **10Ac**, (c) **10Ca**, and (d) **10Cc**. Color coding: C, gray; H, cyan; N, blue; O, red; Cl, green.

interactions. The packing motifs of tetrameric entity observed for **10Ca** and **10Cc** well demonstrate this distinct tendency between these two benzenoid aromatic rings.

As shown in Fig. 7a, the tetrameric entity of **10Ca** is assembled head-to-head in an angular manner having an angle between long molecular axes of about 137.44° viewed down the reciprocal cell axis c^*. At first glance the packing appears to be due to C–H/π interactions in a herringbone arrangement between next-neighbor naphthalenyl rings ($d_{\bullet\cdots\bullet}$=7.311 Å, ∠°=72.46°, shortest $d_{C\cdots C}$=4.430 Å, $d_{C\cdots H}$=3.590 Å, Table 2).[51–53] An examination of the distance between polarized NCH_2 group and adjacent naphthalenyl ring ($d_{H\cdots\bullet}$=4.359 Å; $d_{C\cdots H}$=3.411 Å, Table 2) suggests this packing motif gains more benefit from the NCH_2–π dispersive interactions (inset, Fig. 7a). In addition, the nearby located succinimide rings display intermolecular ArH···O=CN ($d_{H\cdots O}$=2.680 Å) and OCH_3···O=CN ($d_{H\cdots O}$=2.445 Å) close contacts,[54] further fortifying this structural packing motif. Lastly and manifestly, the alignment of tetrameric 1**0Ca** also benefits from intermolecular CH–π interactions of the polarized C–H bonds of methoxy group with naphthalenyl ring, indicated by short OCH_3···Ar and OCH_3···C_{Ar} distances (insett, Fig. 7a, Table 2).[43–46]

The resulting {(HT↔TH)↔(HT↔TH)} tetrameric **10Ca** repeats along the *ab*-plane, which leads to a zigzag band structure. The zigzag molecular bands thereby formed further align with their long axes parallel to one another along the *ab*-plane leading to two-dimensional packing structure in the crystal of **10Ca** (Figs. 7a and S3 in Supplementary data), wherein solvating CH_3CN molecules appear to play the role of filling space in between and linking molecular bands via CN···HC—O and $NCCH_3$···O=C interactions ($d_{N\cdots H}$=2.477 Å and $d_{O\cdots H}$=2.665 Å, respectively, Table S5).

As shown in Fig. 7b, the linear dimers of **10Cc** align in parallel with one another, securely held together by π–π stacking interactions between appended pyrenyl rings; the aromatic rings are coplanar (∠°=0.0°) with a centroid-to-centroid distance of 3.933 Å and a shortest interplanar carbon-to-carbon distance of 3.379 Å (Table 2). This packing motif also gains benefit from NCH_2–π dispersive interactions ($d_{C\cdots H}$=2.997 Å, 3.033 Å). The linearly connected {(HT↔TH)↔(HT↔TH)} tetrameric **10Cc** thereby formed repeats along the *ac*-diagonal leading to tapelike structured polymer. These tapes further pack with their long axes parallel to one another with ArH···O=C, ArH···N, ArH···Cl, QX—H···O=CN, and OCH_3···Cl close contacts (Table 2),[54] resulting in buildup two-dimensional packing structure in the crystal of **10Cc** (Fig. S4a in Supplementary data).

An examination of the three-dimensional packing of tetrameric **10Cc** further reveals an interesting structure motif in the crystal. As shown in Fig. 8, when viewing down crystallographic *c*-axis, tetramers of **10Cc** appear to be piled up on the *ab*-plane with their external BQXO rings stacked against one another face-to-face via the force of π–π stacking interactions (∠°=0.0°, $d_{\bullet\cdots\bullet}$=4.636 Å, $d_{C\cdots C}$=3.309 Å). This packing motif is reinforced by intermolecular CH–π interactions of the polarized C–H bonds of methoxy group with pyrenyl ring and close contacts of QX–H···OCH_3 and OCH_3···OCH_3. Like 1**0Ca**, compound **10Cc** co-crystallized with CH_3CN molecules (Fig. 8), which also appear to play the role of filling space in between and linking molecular tapes via $NCCH_3$···O, CH_3CN···H, and $NCCH_3$···C_{Ar} interactions (Table S5, and Fig. S4b in Supplementary data).

2.3. Proton NMR spectral study

Molecular self-assembly to form tail-to-tail (HT↔TH) dimeric structures in reciprocal clipping manner observed in the solid-state prompted us to undertake the concentration-variant ^{1}H NMR spectral study. As clearly revealed by the side-view drawings for the dimmers of **10A**, **10Ac**, **10Ca**, and **10Cc** shown in Figs. 4 and 5, the

Table 1
Selected structural parameters of monomers and tail-to-tail dimmers in the crystals of **10A**, **10Ac**, **10Ca**, and **10Cc**[a,b,c,d,e,f,g]

	10A	**10Ac**	**10Ca**	**10Cc**
Monomer (wall geometry)	(Divergent)	(Convergent)	(Convergent)	(Convergent)
Average $d_{N\cdots N}/d_{C\cdots C}$	8.21/8.97	7.67/7.22 (7.68/7.37)[h]	7.63/7.12	7.71/7.12
QX//QX ∠ (°)	11.72	6.93 (6.17)[h]	5.83	5.52
QX⋯QX $d_{\bullet\cdots\bullet}$ (Å)	8.465	7.521 (7.562)[h]	7.370	7.384
$OCH_3\cdots$Ar $d_{H\cdots\bullet}$/shortest $d_{H\cdots C}$ (Å)		2.972 (3.146)[h]	2.682/2.715	3.034/2.937
Solvate	AcOEt	None	CH_3CN	CH_3CN
HT↔TH dimer [shape]	[V]	[V]	[₪][i]	[₪][i]
Molecular clipping ∠ (°)	~43	55.12	180	180
QX//[QX]//QX//[QX] ∠ (°)	11.27//21.56//11.27	8.56//3.09//5.43	5.83//0.00//5.83	5.52//0.00//5.52
QX⋯[QX]⋯QX⋯[QX] $d_{\bullet\cdots\bullet}$ (Å)	5.564/5.859/5.564	4.685/4.598/4.515	4.611/4.724/4.611	4.639/4.634/4.639
Shortest QX⋯[QX] $d_{C\cdots C}$ (Å)	3.542/4.734/3.542	3.524/3.840/3.566	3.405/3.656/3.405	3.433/3.615/3.433
Shortest QX⋯[QX] $d_{C\cdots H}$ (Å)	3.361/4.555/3.361	3.450/3.750/3.411		
O–CH⋯N $d_{H\cdots N}$ (Å)	2.632, 2.697	2.706, 2.771; 2.926, 3.014		
O–CH⋯Cl $d_{H\cdots Cl}$ (Å)	2.829	2.900, 3.125; 2.961, 3.206		
QX–H⋯O–CH $d_{H\cdots O}$ (Å)	2.657	2.559, 2.772; 2.699, 2.646	2.772, 2.818; 2.764, 2.908	2.587, 2.591; 2.587, 2.591

[a] QX//QX ∠ and QX⋯QX $d_{\bullet\cdots\bullet}$ denote mean plane angle and centroid-to-centroid distance between quinoxaline walls, respectively.
[b] $d_{x\cdots y}$=distance between non-bonded elements X and Y.
[c] Ar denotes appended aromatic ring.
[d] QX and [QX] denote quinoxaline walls in different molecules.
[e] OCH_3 denotes methoxy group.
[f] HT↔TH denotes tail-to-tail manner of dimer formation.
[g] O–CH denotes oxa-bridge elements.
[h] Values for other conformation.
[i] [₪] denoted the shape of dimer by antiparallel reciprocal clipping.

heteroaryl rings are juxtaposed face-to-face to each other such that QX–Hs (H_a and H_b) are positioned on top of an aromatic ring to experience anisotropic shielding effects and are expected to display upfield shifts. On the other hand, the oxa-bridgehead methine protons (H_c) are located in-plane with the internal sandwiched aromatic ring and thus are deshielded to show downfield shifts.[34,60] We thus embarked on recording the room-temperature ^{1}H NMR spectra (400 MHz) at various concentrations in $CDCl_3$ for **10A**, **10Ab**, and **10Ac**, which are built from same QX-walls, and part of their spectra attributable to QX–Hs (~δ 7.0–9.0) are shown in Fig. 9 (full spectra, see Figs. S5–S7).

The observed concentration-dependent chemical shifts behavior implied that in solution **10A**, **10Ab**, and **10Ac** could self-assemble to form dimeric entities and coexist in equilibrium with their respective monomers, when the concentration was gradually increasing. As shown in Fig. 9a–c, the absorption signals due to H_a, and H_b at the QX ring of **10A**, **10Ab**, and **10Ac** displayed steady shift toward higher magnetic field, whereas the methine protons at oxa-bridgehead (H_c) exhibited slight downfield movement (Figs. S5–S7). Within the concentration ranging from 1×10^{-4} M to 1×10^{-2} M, total changes of chemical shifts for H_a, H_b, and H_c amounting to an average of about 0.073, 0.070, and 0.030 ppm, respectively, were observed. For the remaining protons in **10Ab** and **10Ac**, as shown in Figs. S5–S7, the chemical shifts of protons at appended aryl ring (anthracenyl/pyrenyl), at ring junctions (C–H), OCH_3, and *N*–CH_2 remained essentially unchanged. The succinimidyl hydrogen (*N*–H) for **10A** exhibited downfield movement because of concentration-dependent hydrogen bonding interaction.

The concentration-dependent ^{1}H NMR spectra of BQXO-walled **10Cc** were also recorded and depicted in Figs. 9d and S8 in Supplementary data. Compound **10Cc** exhibits similar trend of changing chemical shift as QX-walled **10Ab** and **10Ac**; its aromatic protons (H_a and H_b) display steady shifts toward higher magnetic field in slightly larger magnitude (Fig. 9d) and the oxa-bridgehead protons (H_c) are somewhat less downfield-shifted (Fig. S8). The corresponding changes of chemical shifts within the concentration range of 1×10^{-4} M to 1×10^{-2} M were 0.12, 0.12, and 0.02 ppm, respectively. Also likewise, the chemical shifts due to protons at appended pyrenyl ring, ring junctions (C–H), methoxy (OCH_3), and amino (*N*–CH_2) remained essentially unchanged (Fig. S8). The overall changing trend of chemical shifts observed in the concentration-dependent ^{1}H NMR spectra of **10A**, **10Ab**, **10Ac**, and **10Cc** suggested that dimers were more likely to be assembled by HT↔TH mode in reciprocal clipping manner (**D**, Fig. 2) but not lined-up in side-by-side fashion, and evidently reverberated the reciprocally clipped dimeric structures found in solid-state (Figs. 4 and 5).

Table 2
Selected structural parameters of head-to-head dimmers in the crystals of **10Ac**, **10Ca**, and **10Cc**[a,b,c,d]

	10Ac	**10Ca**	**10Cc**
TH↔HT dimer (formation of tetramer)			
Ar//[Ar] ∠ (°)	0.50	72.46	0.00
Ar⋯[Ar] $d_{\bullet\cdots\bullet}$ (Å)	3.914	7.311	3.933
Shortest Ar⋯[Ar] $d_{C\cdots C}$ (Å)	3.412	4.430	3.379
N–$CH_2\cdots$Ar $d_{H\cdots\bullet}$ (Å)	4.299; 4.931	4.359	4.406
N–$CH_2\cdots C_{Ar}$ $d_{H\cdots C}$ (Å)	2.856; 2.959	3.441	2.997
NC═O⋯CH_3O $d_{H\cdots O}$ (Å)		2.445	
ArH⋯O═CN $d_{H\cdots O}$ (Å)		2.680	
$OCH_3\cdots$Ar $d_{H\cdots\bullet}$/shortest $d_{H\cdots C}$ (Å)		3.813/2.930	
Interdimeric (inter-tetrameric)			
ArH⋯O═CN $d_{H\cdots O}$ (Å)			2.074
ArH⋯O═C $d_{H\cdots O}$ (Å)			2.672/2.075
ArH⋯N $d_{H\cdots N}$ (Å)			2.741
ArH⋯Cl $d_{H\cdots Cl}$ (Å)			3.025
$OCH_3\cdots$Cl $d_{H\cdots Cl}$ (Å)		2.881	3.092/3.086
ArH⋯O═CN $d_{H\cdots O}$ (Å)	2.446; 2.779		
ArH⋯Cl $d_{H\cdots Cl}$ (Å)	3.041; 3.317		
$OCH_3\cdots$QX $d_{H\cdots\bullet}$/shortest $d_{H\cdots C}$ (Å)	2.654/2.673		
$OCH_3\cdots OCH_3$ $d_{H\cdots O}$ (Å)	2.566		

[a] Refer to Table 1 for similar notations.
[b] Ar and [Ar] denote appended aromatic ring in different molecules.
[c] N–CH_2 denote methylene bonded to succinimide ring.
[d] NC═O denotes carbonyl of succinimide ring.

3. Conclusion

We have synthesized U-shaped septuple-bridged [7,7]orthocyclophanes comprising two sidewalls (phane parts) made of

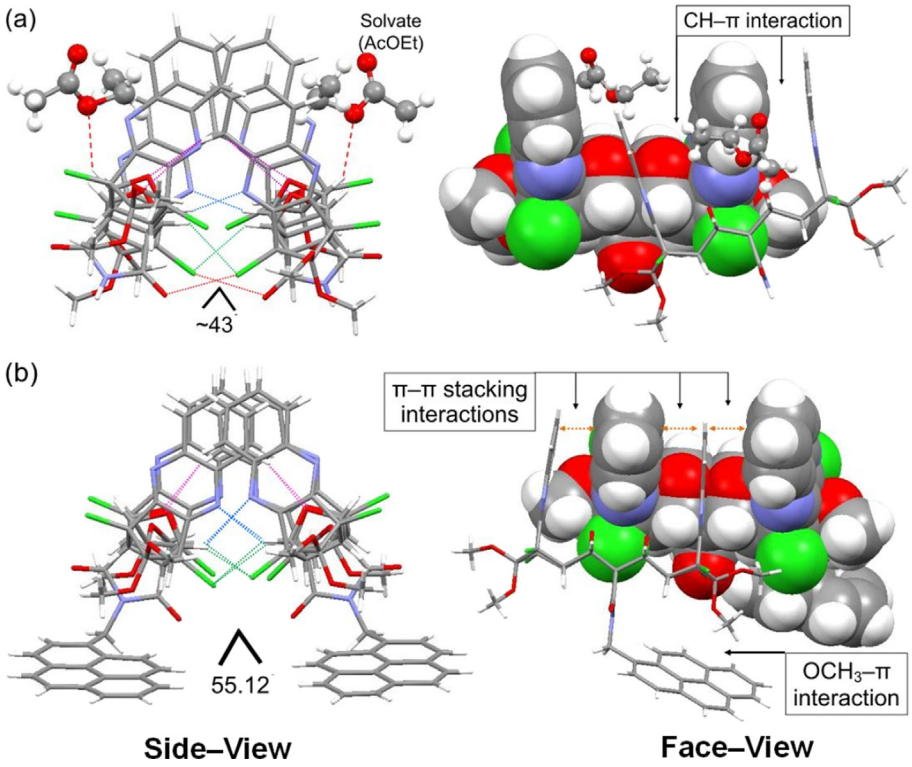

Fig. 4. Two views of packing motifs observed for the tail-to-tail (HT↔TH), V-shaped dimeric entities in the crystal of (a) **10A** with solvate AcOEt in ball-stick style and (b) **10Ac**. The dimeric structures are further secured by close contacts of O–CH···N (blue dot lines), O–CH···Cl (green dot lines), QX–H···O–CH (purple dot lines), and NC=O···Cl (red dot lines). Color coding for atoms: C, gray; H, white; N, blue; O, red; Cl, green.

quinoxaline (QX) or benzoquinoxalinedione (BQXO) rings and a septuple-bridged carbocyclic linker incorporated with succinimide moiety (**10A** and **10C**, Scheme 2), to which a naphthalenyl, anthracenyl or pyrenyl ring is affixed (**10Aa**–**c** and **10Ca**–**c**, Scheme 3). Primarily driven by the force of π–π stacking interaction, these U-shaped [7,7]orthocyclophanes are apt to self-assemble by reciprocal clipping style to form tail-to-tail (HT↔TH) dimeric structure, the QX-walled **10Aa**–**c** in V-shaped (Fig. 4) and **10Ca**–**c** in linear configuration (Fig. 5), as disclosed by X-ray crystal structural analysis. The self-assembly occurrence was further supported by the concentration-variant ^{1}H NMR spectroscopic study. The crystal packing motifs further revealed that the V-shaped dimeric entities of QX-walled **10Ac** formed rhombus-like structured tetramer (Fig. 6) and the linear dimers of BQXO-walled **10Ca** and **10Cc** formed tapelike polymers (Fig. 7) via arene–arene interactions (π–π stacking and C–H/π) between affixed benzenoid rings.

4. Experimental section

4.1. General

Melting points were determined in capillaries and were uncorrected. Infrared (IR) spectra were recorded as a solid suspended in a KBr disk. ^{1}H and ^{13}C NMR spectra were collected using $CDCl_3$ as solvent (unless otherwise specified). Coupling constants are reported in hertz (Hz). The number of attached hydrogens on the carbon atom was determined by the DEPT analysis and is denoted as s (C), d (CH), t (CH_2), and q (CH_3). Mass (MS) spectra were obtained by the FAB mode with 3-nitrobenzyl alcohol (3-NBA) as the matrix. The X-ray crystallography was performed using a Bruker AXS SMART APEX CCD X-ray diffractometer. Graphite monochromatized Mo Kα radiation [λ=0.71073 Å] and temperature of 298(2) K were used. The CCD data were processed with SAINT and the structures were solved by direct method (SHELXS-97) and refined on F^2 by full-matrix least-squares techniques (SHELXL-97). Single crystals were obtained by crystallization in co-solvent system of $CHCl_3$/CH_3CN or $CHCl_3$/AcOEt. Analytical thin-layer chromatography (TLC) was performed on E. Merck silica gel 60 F_{254} plate (0.20 mm). Flash chromatography was performed on E. Merck silica gel (230–400 mesh). All solvents used were either reagent grade or were distilled prior to use.

4.2. Syntheses

4.2.1. General procedure for oxidative removal of N-(4-methoxy benzyl) protecting group. Preparation of N-H-dicarboximides. A solution of *N*-(4-methoxybenzyl)succinimide ring-fused **5**,[34] **1A**,[34] or **1B**[34] (0.5 mmol) and ceric ammonium nitrate (CAN) (5.0 mmol) in CH_3CN/water (75 mL, 2:1 by vol) was heated under N_2 atmosphere at refluxing temperature for a period of time. After the reaction was completed, the mixture was quenched by adding saturated aqueous $NaHCO_3$ solution and extracted with CH_2Cl_2 or EtOAc (2×30 mL). The combined organic phase was washed with water, dried over $MgSO_4$, filtered, and evaporated to give colorless solid residue of **6**, **10A**, or **10C**, respectively.

*4.2.1.1. 4,5,6,7,13,14,15,16-Octachloro-20,20,22,22-tetramethoxy-19,21-dioxaoctacyclo-[8.8.0.1^{2,9}.1^{4,7}.1^{11,18}.1^{13,16}.0^{3,8}.0^{12,17}]docosa-5,14-dien-1,10-dicarboximide (**6**).* Reaction time 12 h; yield 80% (455 mg from 497 mg of **5**). Mp 345 °C (decomp.); IR (KBr, cm^{-1}) 2951 (w), 1725 (s), 1609 (m), 1329 (m), 1271 (m), 1186 (s), 1090 (m), 929 (m), 755 (m); ^{1}H NMR (400 MHz, $CDCl_3$) δ 2.87 (s, 4H), 3.49 (s, 6H), 3.54 (s, 6H), 4.81 (s, 4H), 7.81 (s, 1H); ^{13}C NMR (100 MHz, $CDCl_3$) δ 52.5 (q), 53.0 (q), 53.7 (d), 73.4 (s), 75.5 (s), 80.0 (d), 113.1 (s), 127.4 (s), 171.9 (s); MS (FAB$^+$) *m*/*z* (%) 756 (M$^+$+H, 1.78), 758 (M$^+$+H+2, 2.52), 760 (M$^+$+H+4, 3.09). HRMS (FAB$^+$) calcd for: $C_{26}H_{22}Cl_8NO_8$

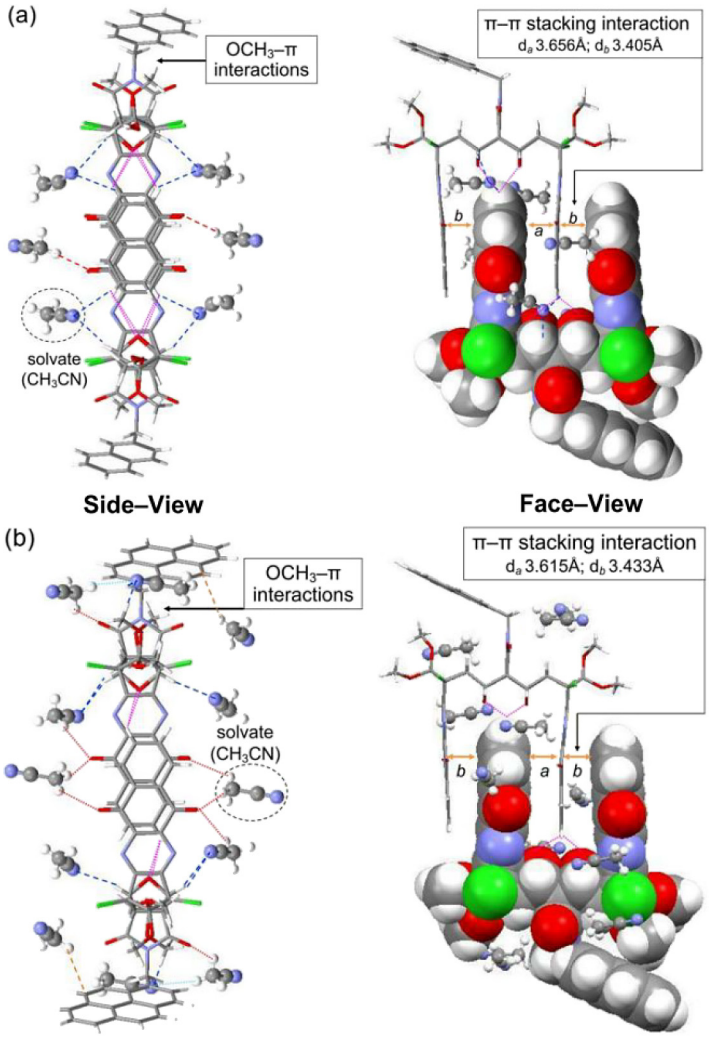

Fig. 5. Two views of packing motifs observed for the tail-to-tail (HT↔TH), linear dimeric entities (antiparallel, clipping angle 180°) in the crystal of (a) **10Ca** fastened by CH_3CN molecules (blue dash lines) and (b) **10Cc** fastened by CH_3CN molecules (red dash lines). The solvate molecules are in ball-stick style. The dimeric structures are further secured by close contacts of QX–H···O–CH (purple dot lines). In **10Cc**, a pair of solvate CH_3CN molecules are associated by CH···N hydrogen bond (2.633 Å, ∠ 166.56°, cyan dash line). Color coding for atoms: C, gray; H, white; N, blue; O, red; Cl, green.

(M^++H): 755.8848; found: 755.8857. Anal. Calcd for $C_{26}H_{21}Cl_8NO_8$: C, 41.14; H, 2.79; N, 1.85; O, 16.86. Found: C, 41.54; H, 3.03; N, 1.59; O, 16.92.

*4.2.1.2. 4,15,21,32-Tetrachloro-36,36,38,38-tetramethoxy-35,37-dioxa-6,13,23,30-tetraazadodecacyclo[16.16.0.1^{2,17}.1^{4,15}.1^{19,34}.1^{21,32}.0^{3,16}.0^{5,14}.0^{7,12}.0^{20,33}.0^{22,31}.0^{24,29}]tetratriaconta-5,7,9,11,13,22,24,26,28,30-decaen-1,18-dicarboximide (**10A**).* Reaction time 12 h; purified by recrystallization from CH_2Cl_2/acetone; yield 68% (288 mg from 500 mg of **1A**). Mp >350 °C; IR (KBr, cm^{-1}) 3298 (br), 2951 (w), 1729 (s), 1515 (w), 1463 (w), 1332 (w), 1191 (s), 1114 (s), 1019 (m), 964 (w), 935 (m), 819 (w), 757 (s), 569 (w); ^{1}H NMR (400 MHz, $CDCl_3$) δ 3.27 (s, 4H), 3.34 (s, 6H), 3.70 (s, 6H), 4.52 (s, 4H), 7.46 (dd, J=3.4, 6.3 Hz, 4H), 7.85 (dd, J=3.4, 6.3 Hz, 4H), 8.63 (s, 1H); ^{13}C NMR (100 MHz, $CDCl_3$) δ 52.5 (q), 52.7 (q), 54.2 (d), 72.4 (s), 79.6 (d), 112.6 (s), 129.15 (d), 129.2 (d), 142.6 (s), 151.6 (s), 172.0 (s); MS (FAB^+) m/z (%) 823 (M^+, 3.66), 824 (M^++H, 3.62), 825 M^++H+1, 5.32), 826 (M^++H+2, 7.21). HRMS (FAB^+) calcd for $C_{38}H_{30}Cl_4N_5O_8$ (M^++H): 824.0848; found: 824.0834. Anal. Calcd for $C_{38}H_{29}Cl_4N_5O_8$: C, 55.29; H, 3.54; N, 8.48. Found: C, 55.58; H, 3.92; N, 8.27.

*4.2.1.3. 4,19,25,40-Tetrachloro-44,44,46,46-tetramethoxy-43,45-dioxa-8,15,29,36-tetraoxo-6,17,27,38-tetraazadodecacyclo[20.20.0.1^{2,21}.1^{4,19}.1^{23,42}.1^{25,40}.0^{3,20}.0^{5,18}.0^{7,16}.0^{9,14}.0^{24,41}.0^{26,39}.0^{28,37}.0^{30,35}]hexatetraconta-5,(7,16),(9,14),10,12,17,26,(28,37),(30,35),31,33,38-dodecaene-1,22-dicarboximide (**10C**).* Reaction time 24 h; purified by flash column chromatography (eluent: CH_2Cl_2/EtOAc); yield 59% (216 mg from 500 mg of **1B**). Mp >350 °C; IR (KBr, cm^{-1}) 3440 (br), 1725 (s), 1687 (s), 1257 (s), 1186 (m), 1119 (m), 1019 (m); ^{1}H NMR (400 MHz, $CDCl_3$) δ 3.92 (s, 4H), 3.33 (s, 6H), 3.71 (s, 6H), 4.44 (s, 4H), 7.75 (dd, J=3.4, 6.3 Hz, 4H), 8.23 (dd, J=3.4, 6.3 Hz, 4H); ^{13}C NMR (125 MHz, acetone-d_6/CS_2) δ 52.8, 54.7, 72.5, 73.3, 79.9, 114.1, 127.7, 133.1, 135.1, 145.8, 156.8, 172.5, 180.5; MS (FAB^+) m/z (%) 983 (M^+, 0.86), 984 (M^++H, 1.74), 985 (M^++H+1, 2.05), 986 (M^++H+2, 3.84). HRMS (FAB^+) calcd for $C_{46}H_{30}Cl_4N_5O_{12}$ (M^++1): 984.0645; found: 984.0640.

*4.2.2. General procedure for mounting N-(arylmethyl) group on N-H-dicarboximides **6**, **10A**, and **10C**. Preparation of N-(arylmethyl)dicarboximides **8a–c**, **10Aa–c**, and **10Ca–c**.* Into a solution of *N*-H-dicarboximide **6** (0.66 mmol), **10A** (0.61 mmol), or **10C** (0.57 mmol) in acetone (50 mL) containing K_2CO_3 (100 mg, 1 mmol) was added **7** (0.8 mmol): [2-(bromomethyl)naphthalene (**7a**), 9-(bromomethyl) anthracene (**7b**), or 1-(bromomethyl)pyrene (**7c**)]. The mixture was heated under reflux for 12 h. Then, acetone was removed and the resulting residue was mixed with CH_2Cl_2 (50 mL) and water (50 mL). The organic phase was separated and washed with brine

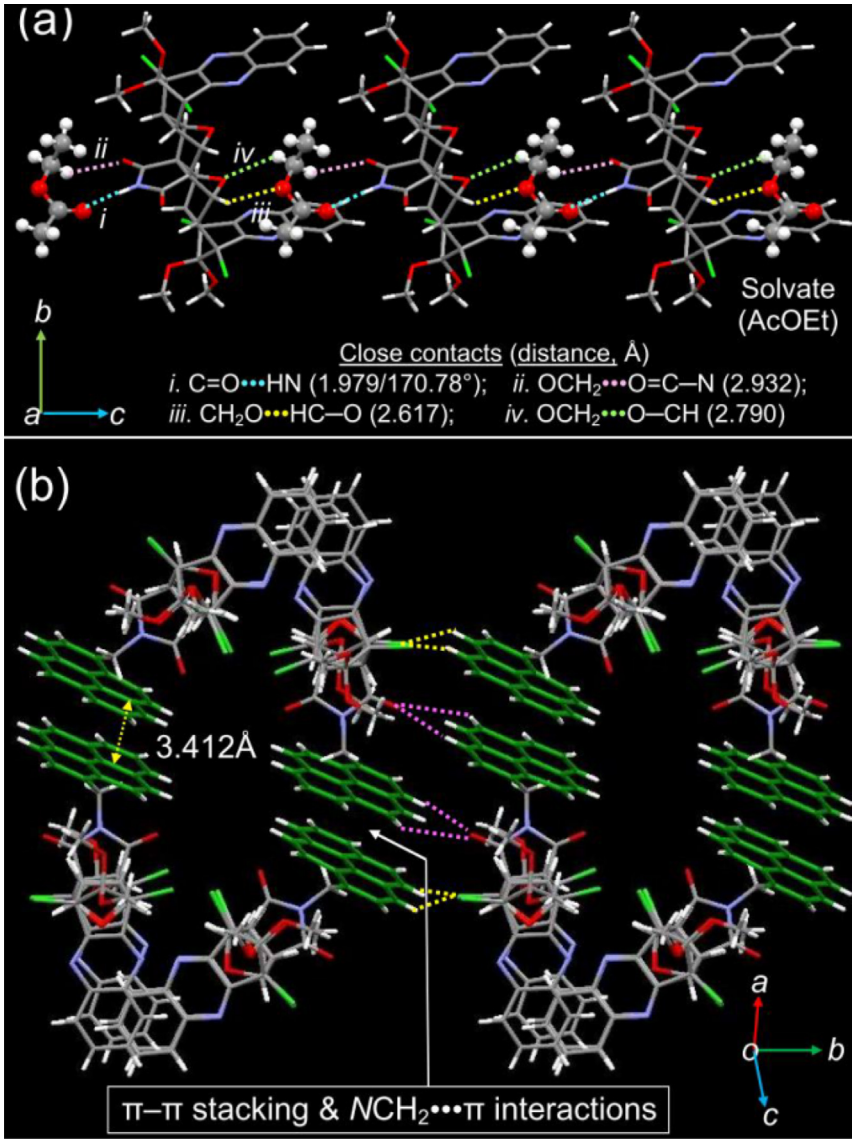

Fig. 6. Packing motifs observed for the V-shaped tail-to-tail (HT↔TH) dimeric units in the crystals of **10A** and **10Ac**: (a) tail-to-head (HT↔HT) assembly of **10A** relayed by solvating AcOEt viewed down crystallographic *a*-axis. Solvate molecules (AcOEt) are in ball-stick style. (b) Rhombus-like structured tetramer {↔(HT↔TH)^2↔}formed by a pair of V-shaped dimers of **10Ac** via π−π stacking interactions between pyrenyl rings. Interdimeric close contacts are indicated by colored dot lines.

(10 mL), dried over $MgSO_4$, and filtered. The filtrate was concentrated to leave a residue of *N*-(arylmethyl)dicarboximide, which was purified via recrystallization from CH_2Cl_2 to give a colorless crystalline of **8a**–**c** or via by flash column chromatography (eluent: CH_2Cl_2/EtOAc) to give pale yellow crystals of **10Aa**–**c** or **10Ca**–**c**.

*4.2.2.1. N-(Naphthalen-2-ylmethyl)-4,5,6,7,13,14,15,16-octachloro-20,20,22,22-tetramethoxy-19,21-dioxaoctacyclo [8.8.0.1^{2,9}.1^{4,7}.1^{11,18}.1^{13,16}.0^{3,8}.0^{12,17}]docosa-5,14-dien-1,10-dicarboximide (**8a**).* Yield 93% (546 mg from 500 mg of **6**). Mp 322 °C (decomp.); IR (KBr, cm^{-1}) 2950 (w), 1708 (s), 1604 (m), 1380 (m), 1326 (m), 1270 (m), 1186 (s), 1125 (m), 1091 (m), 1020 (m), 989 (m), 927 (m), 756 (s); ^{1}H NMR (400 MHz, $CDCl_3$) δ 2.55 (s, 4H), 2.85 (s, 6H), 3.36 (s, 6H), 4.81 (s, 4H), 4.82 (s, 2H), 7.49–7.51 (m, 2H), 7.63 (dd, J=3.4, 6.3 Hz, 1H), 7.82–7.91 (m, 3H), 7.98 (s, 1H); ^{13}C NMR (100 MHz, $CDCl_3$) δ 43.4 (t), 51.2 (q), 52.7 (q), 53.6 (d), 72.2 (s), 75.4 (s), 80.0 (d), 112.9 (s), 126.7 (d), 126.9 (d), 127.0 (s), 127.4 (d), 127.8 (d), 128.6 (d), 129.0 (d), 129.2 (d), 132.3 (s), 133.5 (s), 133.7 (s), 172.5 (s); MS (FAB$^+$) *m*/*z* (%) 896 (M$^+$+H+1, 0.9), 897 (M$^+$+H+2, 0.9), 898 (M$^+$+H+3, 1.47). HRMS (FAB$^+$) calcd for $C_{37}H_{30}Cl_8NO_8$ (M$^+$+1): 895.9474; found: 895.9489. Anal. Calcd for $C_{37}H_{29}Cl_8NO_8$: C, 49.42; H, 3.25; N, 1.56; O, 14.23. Found: C, 49.16; H, 3.49; N, 1.26; O, 14.20.

*4.2.2.2. N-(Anthracen-9-ylmethyl)-4,5,6,7,13,14,15,16-octachloro-20,20,22,22-tetramethoxy-19,21-dioxaoctacyclo[8.8.0.1^{2,9}.1^{4,7}.1^{11,18}.1^{13,16}.0^{3,8}.0^{12,17}]docosa-5,14-dien-1,10-dicarboximide (**8b**).* Yield 91% (570 mg from 500 mg of **6**). Mp >350 °C; IR (KBr, cm^{-1}) 2949 (w), 1707 (s), 1602 (m), 1446 (m), 1327 (m), 1186 (s), 1121 (m), 1027 (m), 925 (m), 757 (s); ^{1}H NMR (400 MHz, $CDCl_3$) δ 2.57 (s, 4H), 2.92 (s, 6H), 3.38 (s, 6H), 4.77 (s, 4H), 5.66 (s, 2H), 7.54 (t, J_1=J_2=7.5 Hz, 2H), 7.68 (t, J_1=J_2=7.5 Hz, 2H), 8.06 (d, J=8.4 Hz, 2H), 8.54 (s, 1H), 8.69 (d, J=8.4 Hz, 2H); ^{13}C NMR (100 MHz, $CDCl_3$) δ 37.4 (t), 51.3 (q), 52.7 (q), 53.5 (d), 71.9 (s), 75.4 (s), 80.2 (d), 112.9 (s), 124.4 (s), 124.5 (d), 125.6 (d), 127.4 (s), 127.4 (d), 129.5 (d), 129.9 (d), 131.6 (s), 131.7 (s), 173.2 (s); MS (FAB$^+$) *m*/*z* (%) 944 (M$^+$, 1.61), 945 (M$^+$+H, 2), 946 (M$^+$+H+1, 3.04), 947 (M$^+$+H+2, 3.11). HRMS (FAB$^+$) calcd for $C_{41}H_{32}Cl_8NO_8$ (M$^+$+1): 945.9631; found: 945.9645. Anal. Calcd for $C_{41}H_{31}Cl_8NO_8$: C, 51.87; H, 3.29; N, 1.48; O, 13.48. Found: C, 51.47; H, 2.98; N, 1.56; O, 13.55.

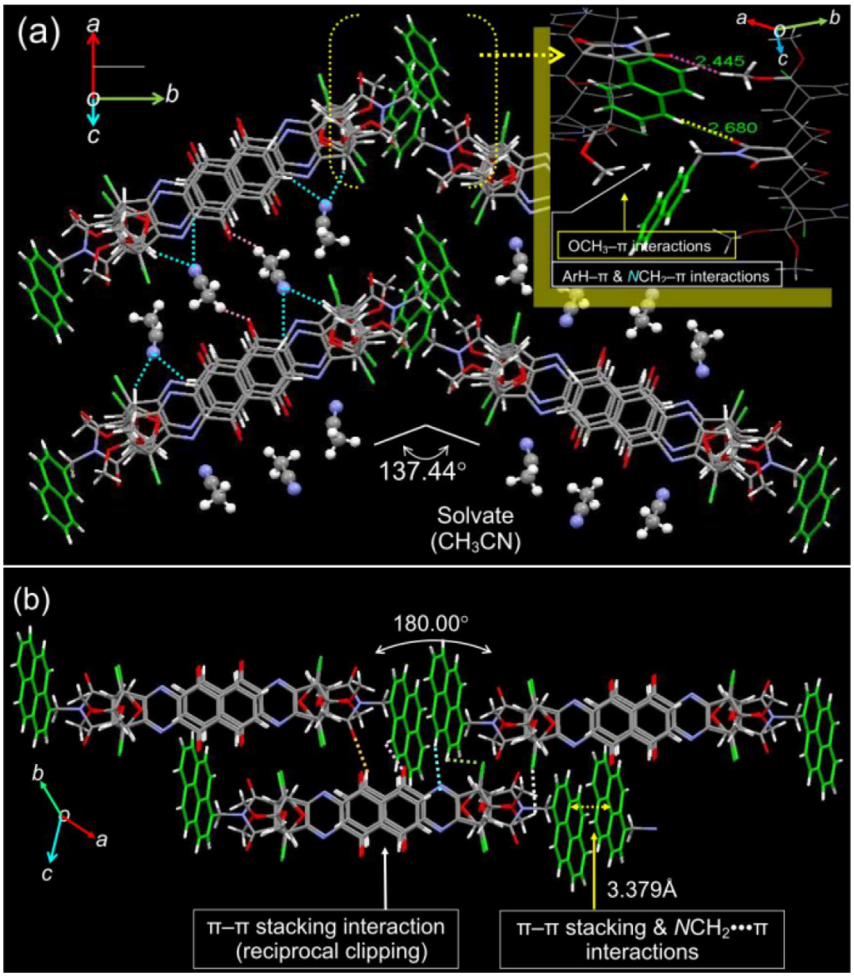

Fig. 7. Interdimeric packing motifs observed for the linear tail-to-tail (HT↔TH) dimeric units leading to head-to-head {(HT↔TH)↔(HT↔TH)} tetrameric entities and subsequent packing into two-dimensional structures in the crystals of **10Ca** and **10Cc**. Interdimeric close contacts are indicated by colored dot lines. (a) Assembly of tetrameric **10Ca**, driven by C–H/π and NCH_2–π dispersive interactions (inset), in an angular manner (137.44°), viewed down reciprocal cell axis c^*, with CH_3CN molecules (in ball-stick style) as linking agents between molecular bands. (b) Packing structure of linearly tetrameric **10Cc** assembled by π–π stacking interactions between pyrenyl rings (on *ac*-plane). Solvate molecules (CH_3CN) in **10Cc** are hidden for clarity.

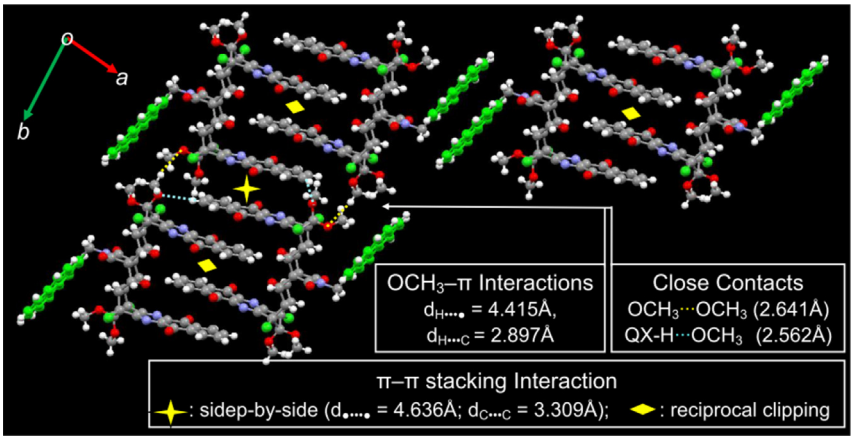

Fig. 8. Interdimeric packing motifs observed for the linear tail-to-tail (HT↔TH) dimeric **10Cc** viewed down crystallographic *c*-axis (on *ab*-plane) showing π–π stacking interactions (✦) between flanking BQXO-walls (∠°=0.0°), OCH_3–π interactions, and interdimeric close contacts of OCH_3···OCH_3 and QX—H···OCH_3. Solvate molecules (CH_3CN) are hidden for clarity.

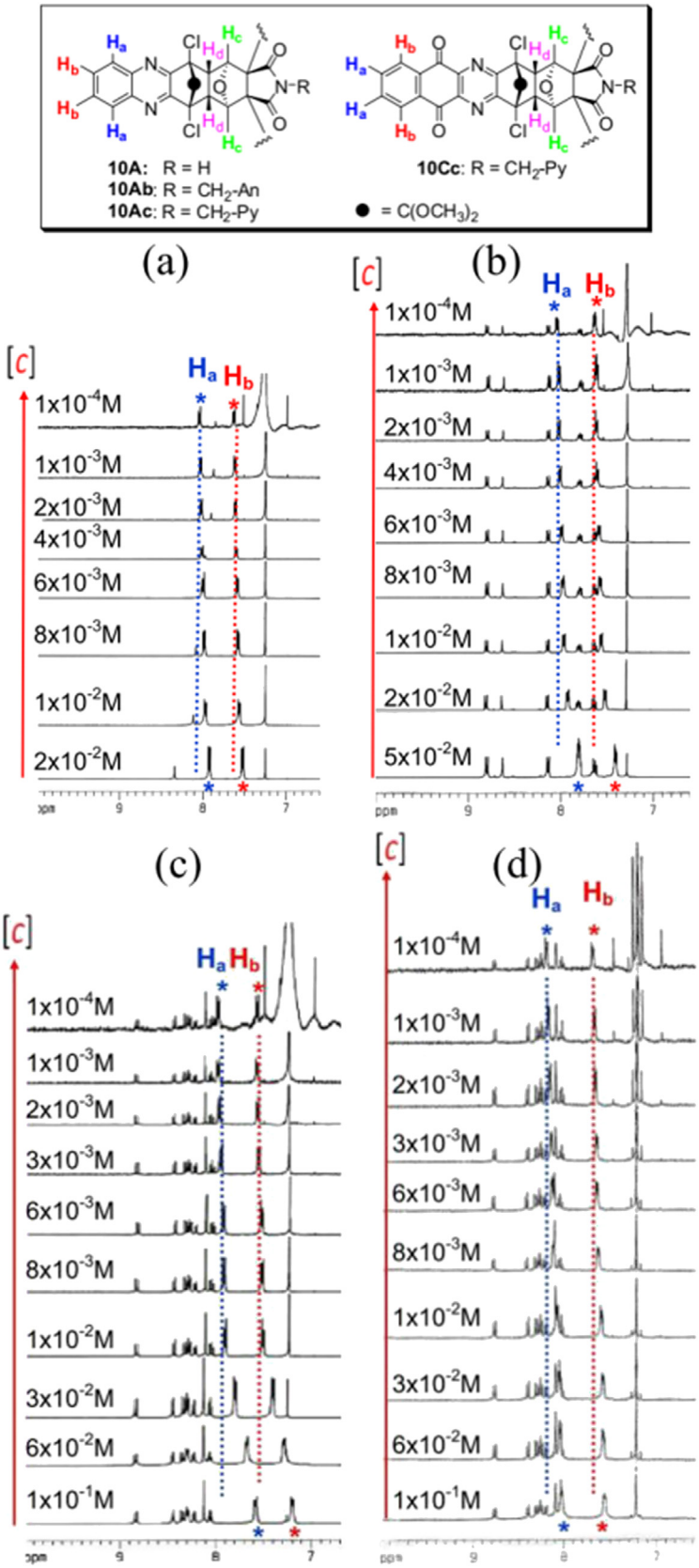

Fig. 9. Part of concentration-variant ^{1}H NMR spectra of (a) **10A**, (b) **10Ab**, (c) **10Ac**, and (d) **10Cc** in the range from δ 7.0 to 9.0 ($CDCl_3$, 400 MHz).

*4.2.2.3. N-(Pyren-1-ylmethyl)-4,5,6,7,13,14,15,16-octachloro-20,20,22,22-tetramethoxy-19,21-dioxaoctacyclo[8.8.0.0^{1}^{2,9}.1^{4,7}.1^{11,18}.1^{13,16}.0^{3,8}.0^{12,17}]docosa-5,14-dien-1,10-dicarboximide (**8c**).* Yield 91% (597 mg from 500 mg of **6**). Mp >350 °C; IR (KBr, cm^{-1}) 2949 (w), 1708 (s), 1604 (m), 1381 (m), 1330 (m), 1186 (s), 1120 (m), 1091 (m), 927 (m), 849 (m), 756 (s); ^{1}H NMR (400 MHz, $CDCl_3$) δ 2.52 (s, 4H), 2.53 (s, 6H), 3.23 (s, 6H), 4.79 (s, 4H), 5.41 (s, 2H), 8.04–8.12 (m, 3H), 8.21–8.24 (m, 4H), 8.38 (d, *J*=9.4 Hz, 1H), 8.78 (d, *J*=9.4 Hz, 1H); ^{13}C NMR (100 MHz, $CDCl_3$) δ 41.3 (t), 50.9 (q), 52.0 (q), 53.6 (d), 72.1 (s), 75.3 (s), 80.1 (d), 112.8 (s), 122.9 (s), 124.9 (s), 125.1 (s), 125.82 (s), 125.84 (d), 126.4 (d), 127.3 (s), 127.4 (d), 127.6 (d), 128.4 (d), 129.3 (d), 129.7 (d), 130.0 (s), 131.3 (s), 132.0 (s), 172.9 (s); MS (FAB$^+$) *m*/*z* (%) 968 (M$^+$, 2.71), 969 (M$^+$+H, 3.97), 967 (M$^+$+H+1, 4.37), 968 (M$^+$+H+2, 4.38). HRMS (FAB$^+$) calcd for $C_{43}H_{32}Cl_8NO_8$ (M$^+$+1): 969.9631; found: 969.9551. Anal. Calcd for $C_{43}H_{31}Cl_8NO_8$: C, 53.06; H, 3.21; N, 1.44. Found: C, 53.53; H, 3.09; N, 1.28.

*4.2.2.4. N-(Naphthalen-2-ylmethyl)-4,15,21,32-tetrachloro-36,36,38,38-tetramethoxy-35,37-dioxa-6,13,23,30-tetraazadodecacyclo[16.16.0.0^{1}^{2,17}.1^{4,15}.1^{19,34}.1^{21,32}.0^{3,16}.0^{5,14}.0^{7,12}.0^{20,33}.0^{22,31}.0^{24,29}]tetratriaconta-5,7,9,11,13,22,24,26,28,30-decaen-1,18-dicarboximide (**10Aa**).* Yield 93% (549 mg from 500 mg of **10A**). Mp >350 °C; IR (KBr, cm^{-1}) 2950 (w), 1709 (s), 1514 (w), 1460 (w), 1336 (m), 1193 (s), 1123 (s), 1027 (w), 996 (m), 966 (w), 818 (w), 756 (s); ^{1}H NMR (400 MHz, $CDCl_3$) δ 2.92 (s, 4H), 3.03 (s, 6H), 3.20 (s, 6H), 4.43 (s, 4H), 4.94 (s, 4H), 7.50–7.57 (m, 6H), 7.72 (d, *J*=8.0 Hz, 1H), 7.89–7.92 (m, 5H), 7.98(d, *J*=8.0, 2H), 8.07 (s, 1H); ^{13}C NMR (100 MHz, $CDCl_3$) δ 43.4 (t), 51.7 (q), 52.4 (q), 54.0 (d), 71.1 (s), 72.3 (s), 79.6 (d), 112.3 (s), 126.8 (d), 127.0 (d), 127.1 (d), 127.8 (d), 128.7 (d), 129.1 (d), 129.1 (d), 129.4 (d), 129.5 (d), 132.2 (s), 133.5 (s), 133.8 (s), 142.5 (s), 151.6 (s), 172.3 (s); MS (FAB$^+$) *m*/*z* (%) 963 (M$^+$, 0.95), 964 (M$^+$+H, 1.95), 965 (M$^+$+H+1, 1.34), 966 (M$^+$+H+2, 2.66). HRMS (FAB$^+$) calcd for $C_{49}H_{38}Cl_4N_5O_8$ (M$^+$+1): 964.1469; found: 964.1472. Anal. Calcd for $C_{49}H_{37}Cl_4N_5O_8$: C, 60.95; H, 3.86; N, 7.25; O, 13.25. Found: C, 60.71; H, 3.72; N, 7.34; O, 13.44.

*4.2.2.5. N-(Anthracen-9-ylmethyl)-4,15,21,32-tetrachloro-36,36,38,38-tetramethoxy-35,37-dioxa-6,13,23,30-tetraazadodecacyclo[16.16.0.0^{1}^{2,17}.1^{4,15}.1^{19,34}.1^{21,32}.0^{3,16}.0^{5,14}.0^{7,12}.0^{20,33}.0^{22,31}.0^{24,29}]tetratriaconta-5,7,9,11,13,22,24,26,28,30-decaen-1,18-dicarboximide (**10Ab**).* Yield 92% (566 mg from 500 mg of **10A**). Mp >350 °C; IR (KBr, cm^{-1}) 2950 (w), 1710 (s), 1447 (w), 1328 (m), 1192 (s), 1117 (s), 995 (m), 757 (s); ^{1}H NMR (400 MHz, $CDCl_3$) δ 2.93 (s, 4H), 3.13 (s, 6H), 3.21 (s, 6H), 4.37 (s, 4H), 5.78 (s, 2H), 7.56–7.64 (dd, *J*=3.4, 6.3 Hz, 4H), 7.73–7.80 (m, 4H), 7.93–8.0 (dd, *J*=3.4, 6.3 Hz, 4H), 8.09 (d, *J*=3.4 Hz, 2H), 8.60 (s, 1H), 8.74 (d, 2H); ^{13}C NMR (100 MHz, $CDCl_3$) δ 41.4 (t), 51.9 (q), 52.4 (q), 53.9 (d), 70.8 (s), 72.3 (s), 79.9 (d), 112.4 (s), 124.4 (d), 124.4 (d), 125.7 (d), 127.6 (d), 129.3 (d), 129.6 (d), 129.6 (d), 130.1 (d), 131.7 (s), 131.7 (s), 142.6 (s), 151.7 (s), 172.9 (s); MS (FAB$^+$) *m*/*z* (%) 1013 (M$^+$, 2.26), 1014 (M$^+$+H, 4.4), 1015 (M$^+$+H+1, 4.43), 1016 (M$^+$+H+2, 6.07). HRMS (FAB$^+$) calcd for $C_{53}H_{40}Cl_4N_5O_8$ (M$^+$+H): 014.1626; found: 1014.1639. Anal. Calcd for $C_{53}H_{39}Cl_4N_5O_8$: C, 62.67; H, 3.87; N, 6.89. Found: C, 62.70; H, 3.90; N, 6.44.

*4.2.2.6. N-(Pyren-1-ylmethyl)-4,15,21,32-tetrachloro-36,36,38,38-tetramethoxy-35,37-dioxa-6,13,23,30-tetraazadodecacyclo[16.16.0.0^{1}^{2,17}.1^{4,15}.1^{19,34}.1^{21,32}.0^{3,16}.0^{5,14}.0^{7,12}.0^{20,33}.0^{22,31}.0^{24,29}]tetratriaconta-5,7,9,11,13,22,24,26,28,30-decaen-1,18-dicarboximide (**10Ac**).* Yield 95% (598 mg from 500 mg of **10A**). Mp >350 °C; IR (KBr, cm^{-1}) 2950 (w), 1709 (s), 1333 (m), 1192 (s), 1118 (s), 995 (m), 912 (m), 848 (m), 757 (s); ^{1}H NMR (400 MHz, $CDCl_3$) δ 2.71 (s, 6H), 2.86 (s, 4H), 3.11 (s, 6H), 4.55 (s, 4H), 5.52 (s, 2H), 7.20 (dd, *J*=3.4, 6.3 Hz, 4H), 7.58 (dd, *J*=3.4, 6.3 Hz, 4H), 8.06–8.36 (m, 5H), 8.45 (d, *J*=3.4 Hz, 1H), 8.84 (d, *J*=3.4 Hz, 1H); ^{13}C NMR (100 MHz, $CDCl_3$) δ 41.4 (t), 51.5 (q), 52.3 (q), 54.0 (d), 71.0 (s), 72.2 (s), 79.8 (d), 112.3 (s), 122.9 (d), 125.2 (d), 125.4 (s), 125.9 (d), 126.0 (d), 126.5 (d), 127.5 (s), 127.5 (d), 128.5 (d), 129.4 (d), 129.5 (d), 129.6 (d), 129.8 (s), 130.2 (d), 131.1 (s), 131.3 (s), 132.2 (s), 142.6 (s), 151.7 (s), 172.6 (s); MS (FAB$^+$) *m*/*z* (%)1039 (M$^+$+H+1, 4.02), 1040 (M$^+$+H+2, 25.99). HRMS (FAB$^+$) calcd for $C_{55}H_{40}Cl_4N_5O_8$ (M$^+$+H): 1038.1626; found: 1038.1635.

*4.2.2.7. N-(Naphthalen-2-ylmethyl)-4,19,25,40-tetrachloro-44,44,46,46-tetramethoxy-43,45-dioxa-8,15,29,36-tetraoxo-6,17,27,38-tetraazadodecacyclo[20.20.0.0^{1}^{2,21}.1^{4,19}.1^{23,42}.1^{25,40}.0^{3,20}.0^{5,18}.0^{7,16}.0^{9,14}.0^{24,41}.0^{26,39}.0^{28,37}.0^{30,35}]hexatetraconta-5,(7,16),(9,14),10,12,17,26,(28,37),(30,35),31,33,38-dodecaene-1,22-dicarboximide (**10Ca**).* Yield 93% (455 mg from 500 mg of **10C**). Mp >350 °C; IR (KBr, cm^{-1}) 2952 (w), 1711 (s), 1592 (m), 1379 (m), 1257 (s), 1191 (m), 1118 (m), 1003 (m), 939 (w), 754 (m); ^{1}H NMR (400 MHz, $CDCl_3$) δ 2.91 (s, 4H), 3.01 (s, 6H), 3.22 (s, 6H), 4.45 (s, 4H), 4.93 (s, 4H), 7.51–7.55 (m, 6H), 7.71 (d, *J*=8.3 Hz, 1H), 7.89–7.97 (m, 7H), 8.05 (s, 1H); ^{13}C NMR (100 MHz, $CDCl_3$) δ 43.5 (t), 52.0 (q), 52.6 (q), 54.0 (d), 70.9 (s), 72.1 (s), 80.0 (d), 113.4 (s), 126.8 (d), 127.0 (d), 127.1 (d), 127.6 (d), 127.8 (d), 128.7 (d), 129.1 (d), 129.5 (d), 132.0 (s), 132.2 (s), 133.6 (s), 133.7 (s), 134.7 (d), 145.0 (s), 156.8 (s), 171.5 (s), 180.4 (s); MS (FAB$^+$) *m*/*z* (%) 1124 (M$^+$+H, 7.43), 1126 (M$^+$+H+2, 20.29). HRMS (FAB$^+$) calcd for $C_{57}H_{38}Cl_4N_5O_{12}$ (M$^+$+H): 1124.1266; found: 1124.1260.

*4.2.2.8. N-(Anthracen-9-ylmethyl)-4,19,25,40-tetrachloro-44,44,46,46-tetramethoxy-43,45-dioxa-8,15,29,36-tetraoxo-6,17,27,38-tetraazadodecacyclo[20.20.0.0^{1}^{2,21}.1^{4,19}.1^{23,42}.1^{25,40}.0^{3,20}.0^{5,18}.0^{7,16}.0^{9,14}.0^{24,41}.0^{26,39}.0^{28,37}.0^{30,35}]hexatetraconta-5,(7,16),(9,14),10,12,17,26,(28,37),(30,35),31,33,38-dodecaene-1,22-dicarboximide (**10Cb**).* Yield 93% (554 mg from 500 mg of **10C**). Mp >350 °C; IR (KBr, cm^{-1}) 3000 (w), 1708 (s), 1685 (s), 1590 (m), 1446 (m), 1378 (m), 1254 (s), 1183 (m), 1117 (m), 1000 (m), 936 (m), 746 (s). ^{1}H NMR (400 MHz, $CDCl_3$) δ 2.94 (s, 4H), 3.14 (s, 6H), 3.23 (s, 6H), 4.40 (s, 4H), 5.78 (s, 2H), 7.58–7.62 (m, 6H), 7.77 (dd, *J*=9.4, 8.2 Hz, 2H), 8.05–8.07 (m, 4H), 8.11 (d, *J*=8.4 Hz, 2H), 8.60 (s, 1H), 8.73 (d, *J*=9.1 Hz, 2H); ^{13}C NMR (100 MHz, $CDCl_3$) δ 37.5 (t), 52.2 (q), 52.6 (q), 54.0 (d), 70.6 (s), 72.2 (s), 80.0 (d), 113.5 (s), 124.1 (s), 124.3 (d), 125.7 (d), 127.7 (d), 127.7 (d), 129.6 (d), 130.1 (d), 131.6 (s), 131.7 (s), 132.4 (d), 134.8 (s), 145.1 (s), 156.9 (s), 172.2 (s), 180.6 (s); MS (FAB$^+$) *m*/*z* (%) 1173 (M$^+$, 0.61), 1174 (M$^+$+H, 1.11), 1175 (M$^+$+H+1, 1.03), 1176 (M$^+$+H+2, 1.44). HRMS (FAB$^+$) calcd for $C_{61}H_{40}Cl_4N_5O_{12}$ (M$^+$+H): 1174.1412; found: 1174.1454.

*4.2.2.9. N-(Pyren-1-ylmethyl)-4,19,25,40-tetrachloro-44,44,46,46-tetramethoxy-43,45-dioxa-8,15,29,36-tetraoxo-6,17,27,38-tetraazadodecacyclo[20.20.0.0^{1}^{2,21}.1^{4,19}.1^{23,42}.1^{25,40}.0^{3,20}.0^{5,18}.0^{7,16}.0^{9,14}.0^{24,41}.0^{26,39}.0^{28,37}.0^{30,35}]hexatetraconta-5,(7,16),(9,14),10,12,17,26,(28,37),(30,35),31,33,38-dodecaene-1,22-dicarboximide (**10Cc**).* Yield 96% (577 mg from 500 mg of **10C**). Mp >350 °C; IR (KBr, cm^{-1}) 2952 (w), 1712 (s), 1687 (s), 1592 (s), 1445 (m), 1380 (m), 1256 (s), 1191 (m), 1003 (m), 849 (m), 755 (m); ^{1}H NMR (400 MHz, $CDCl_3$) δ 2.66 (s, 6H), 2.88 (s, 4H), 3.08 (s, 6H), 4.41 (s, 4H), 5.51 (s, 2H), 7.65 (dd, *J*=9.2, 5.8, Hz, 4H), 8.06–8.13 (m, 7H), 8.22–8.35 (m, 4H), 8.44 (d, *J*=8 Hz, 1H), 8.81 (d, *J*=9.4 Hz, 1H); ^{13}C NMR (100 MHz, $CDCl_3$) δ 41.8 (t), 51.7 (q), 52.5 (q), 54.0 (d), 70.9 (s), 72.2 (s), 79.9 (d), 113.5 (s), 122.7 (d), 125.0 (s), 125.2 (s), 125.4 (s), 126.0 (d), 126.6 (d), 127.3 (d), 127.5 (s), 127.7 (d), 129.7 (d), 129.8 (d), 130.4 (d), 131.1 (d), 131.3 (s), 132.2 (s), 132.5 (s), 134.8 (d), 145.2 (s), 156.8 (s), 171.9 (s), 180.7 (s); MS (FAB$^+$) *m*/*z* (%) 1197 (M$^+$, 1.16), 1198 (M$^+$+H, 1.79), 1199 (M$^+$+H+1, 3.28), 1200 (M$^+$+H+2, 5.24). HRMS (FAB$^+$) calcd for $C_{63}H_{39}Cl_4N_5O_{12}$ (M$^+$+H): 1198.1422; found: 1198.1423.

Acknowledgements

The financial support from the Ministry of Science and Technology of Taiwan is gratefully acknowledged.

Supplementary data

Figures of two-dimensional network of crystals, figures of concentration-variant ^{1}H NMR spectra, tables of crystal data and structure refinement (with cif files), table of selected close contacts involving solvate, and ^{1}H and ^{13}C NMR spectra for the newly synthesized compounds. Supplementary data associated with this article can be found in the online version, at http://dx.doi.org/10.1016/j.tet.2015.06.046.

References and notes

1. Steed, J. W.; Atwood, J. L. *Supramolecular Chemistry*, 2nd ed..; John Wiley & Sons: New York, NY, 2009.
2. *The Importance of Pi-Interactions in Crystal Engineering: Frontiers in Crystal Engineering*; Tiekink, E. R. T., Zukerman-Schpector, J., Eds.; John Wiley & Sons: Chichester, West Sussex, 2012.
3. Salonen, L. M.; Ellermann, M.; Diederich, F. *Angew. Chem., Int. Ed.* **2011**, *50*, 4808–4842.
4. Meyer, E. A.; Castellano, R. K.; Diederich, F. *Angew. Chem., Int. Ed.* **2003**, *42*, 1210–1250.
5. Riley, K. E.; Hobza, P. *Acc. Chem. Res.* **2013**, *46*, 927–936.
6. Hoeben, F. J. M.; Jonkheijm, P.; Meijer, E. W.; Schenning, A. P. H. J. *Chem. Rev.* **2005**, *105*, 1491–1546.
7. Hunter, C. A.; Lawson, K. R.; Perkins, J.; Urch, C. J. *J. Chem. Soc., Perkin Trans. 2* **2001**, 651–669.
8. Zhang, Z.; Luo, Y.; Chen, J.; Dong, S.; Yu, Y.; Ma, Z.; Huang, F. *Angew. Chem., Int. Ed.* **2011**, *50*, 1397–1401.
9. Yao, Y.; Xue, M.; Chen, J.; Zhang, M.; Huang, F. *J. Am. Chem. Soc.* **2012**, *134*, 15712–15715.
10. Yao, Y.; Chi, X.; Zhou, Y.; Huang, F. *Chem. Sci.* **2014**, *5*, 2778–2782.
11. Kinbara, K.; Aida, T. *Chem. Rev.* **2005**, *105*, 1377–1400.
12. *Organic Structure Design: Applications in Optical and Electronic Devices*; Chow, T. J., Ed.; Pan Stanford: Singapore, 2014.
13. Ghosh, S.; Mukherjee, P. S. *J. Org. Chem.* **2006**, *71*, 8412–8416.
14. Wang, B.-Y.; Žujović, T.; Turner, D. A.; Hadad, C. M.; Badjić, J. D. *J. Org. Chem.* **2012**, *77*, 2675–2688.
15. Chou, T.-C.; Hwa, C.-L.; Lin, J.-J.; Liao, K.-C.; Tseng, J.-C. *J. Org. Chem.* **2005**, *70*, 9717–9726.
16. Han, Y.; Meng, Z.; Ma, Y.-X.; Chen, C. F. *Acc. Chem. Res.* **2014**, *47*, 2026–2040.
17. Yang, J.-S.; Liu, C.-P.; Lin, B.-C.; Tu, C.-W.; Lee, G.-H. *J. Org. Chem.* **2002**, *67*, 7343–7354.
18. Hardouin-Lerouge, M.; Hudhomme, P.; Sallé, M. *Chem. Soc. Rev.* **2011**, *40*, 30–43.
19. Harmata, M. *Acc. Chem. Res.* **2004**, *37*, 862–873.
20. Kobryn, L.; Henry, W. P.; Fronczek, F. R.; Sygula, R.; Sygula, A. *Tetrahedron Lett.* **2009**, *50*, 7124–7127.
21. Legouin, B.; Gayral, M.; Uriac, P.; Cupif, J. F.; Levoin, N.; Toupet, L.; van de Weghe, P. *Eur. J. Org. Chem.* **2010**, *28*, 5503–5508.
22. Harmata, M.; Kahraman, M.; Tyagarajan, S.; Barnes, C. L.; Welch, C. J. In *Molecular Recognition and Inclusion*; Coleman, A. W., Ed.; Kluwer: Dordrecht, The Netherlands, 1998; pp 109–116.
23. Harmata, M.; Murray, T. *J. Org. Chem.* **1989**, *54*, 3761–3763.
24. Veale, E. B.; Frimannsson, D. O.; Lawler, M.; Gunnlaugsson, T. *Org. Lett.* **2009**, *11*, 4040–4043.
25. D'Souza, L. J.; Maitra, U. *J. Org. Chem.* **1996**, *61*, 9494–9502.
26. Potluri, V. K.; Maitra, U. *J. Org. Chem.* **2000**, *65*, 7764–7769.
27. Klärner, F.-G.; Schrader, T. *Acc. Chem. Res.* **2013**, *46*, 967–978.
28. Branchi, B.; Balzani, V.; Ceroni, P.; Kuchenbrandt, M. C.; Klärner, F.-G.; Bläser, D.; Boese, R. *J. Org. Chem.* **2008**, *73*, 5839–5851.
29. Klärner, F.-G.; Burkert, U.; Kamieth, M.; Boese, R. *J. Phys. Org. Chem.* **2000**, *13*, 604–611.
30. Lagona, J.; Mukhopadhyay, P.; Chakrabarti, S.; Isaacs, L. *Angew. Chem., Int. Ed.* **2005**, *44*, 4844–4870.
31. Conn, M. M.; Rebek, J., Jr. *Chem. Rev.* **1997**, *97*, 1647–1668.
32. Rowan, A. E.; Elemans, J. A. A. W.; Nolte, R. J. M. *Acc. Chem. Res.* **1999**, *32*, 995–1006.
33. Chou, T.-C.; Liao, K.-C.; Lin, J.-J. *Org. Lett.* **2005**, *7*, 4843–4846.
34. Chou, T.-C.; Lin, K.-C.; Wu, C.-A. *Tetrahedron* **2009**, *65*, 10243–10257.
35. Chou, T.-C.; Liao, K.-C. *Tetrahedron* **2011**, *67*, 236–249.
36. Khan, F. A.; Prabhudas, B.; Dash, J. *J. Prakt. Chem.* **2000**, *342*, 512–517.
37. Head, N. J.; Oliver, A. M.; Look, K.; Lokan, N. R.; Jones, G. A.; Paddon-Row, M. N. *Angew. Chem., Int. Ed.* **1999**, *38*, 3219–3222.
38. Khan, F. A.; Das, B. P.; Dash, J.; Sahu, N. *J. Am. Chem. Soc.* **2000**, *122*, 9558–9559.
39. Etzkorn, M.; Timmerman, J. C.; Brooker, M. D.; Yu, X.; Gerken, M. *Beilstein J. Org. Chem.* **2010**, *39*.
40. DeBlase, C. R.; Finke, R. T.; Porras, J. A.; Tanski, J. M.; Nadeau, J. M. *J. Org. Chem.* **2014**, *79*, 4312–4321.
41. Sridharan, V.; Menéndez, J. C. *Chem. Rev.* **2010**, *110*, 3805–3849.
42. Williams, R. M.; Sabol, M. R.; Kim, H.-d.; Kwast, A. *J. Am. Chem. Soc.* **1991**, *113*, 6621–6633.
43. Carroll, W. R.; Zhao, C.; Smith, M. D.; Pellechia, P. J.; Shimizu, K. D. *Org. Lett.* **2011**, *13*, 4320–4323.
44. Nijamudheen, A.; Jose, D.; Shine, A.; Datta, A. *J. Phys. Chem. Lett.* **2012**, *3*, 1493–1496.
45. Kim, E.; Paliwal, S.; Wilcox, C. S. *J. Am. Chem. Soc.* **1998**, *120*, 11192–11193.
46. Wang, Z.-G.; Zhou, B.-H.; Chen, Y.-F.; Yin, G.-D.; Li, Y.-T.; Wu, A.-X.; Isaacs, L. *J. Org. Chem.* **2006**, *71*, 4502–4508.
47. McGuaghey, G. B.; Gagné, M.; Rappé, A. K. *J. Biol. Chem.* **1998**, *273*, 15458–15463.
48. Gung, B. W.; Patel, M.; Xue, X. *J. Org. Chem.* **2005**, *70*, 10532–10537.
49. Carroll, W. R.; Pellechia, P.; Shimizu, K. D. *Org. Lett.* **2008**, *10*, 3547–3550.
50. Hinoue, T.; Shigenoi, Y.; Sugino, M.; Mizobe, Y.; Hisaki, I.; Miyata, M.; Tohnai, N. *Chem.—Eur. J.* **2012**, *18*, 4634–4643.
51. Chelli, R.; Gervasio, F. L.; Procacci, P.; Schettino, V. *J. Am. Chem. Soc.* **2002**, *124*, 6133–6143.
52. Jennings, W. B.; Farrell, B. M.; Malone, J. F. *Acc. Chem. Res.* **2001**, *34*, 885–894.
53. Desiraju, G. *Acc. Chem. Res.* **2002**, *35*, 565–573.
54. Steiner, T. *Angew. Chem., Int. Ed.* **2002**, *41*, 48–76.
55. Desiraju, G. *Acc. Chem. Res.* **1996**, *29*, 441–449.
56. MacGillivray, L. R. *J. Org. Chem.* **2008**, *73*, 3311–3317.
57. Metrangolo, P.; Resnati, G. *Chem.—Eur. J.* **2001**, *7*, 2511–2519.
58. Pigge, F. C.; Vangala, V. R.; Swenson, D. C.; Rath, N. P. *Cryst. Growth Des.* **2010**, *10*, 224–231.
59. Liang, Z.; Tang, Q.; Liu, J.; Li, J.; Yan, F.; Miao, Q. *Chem. Mater.* **2010**, *22*, 6438–6443.
60. Bovey, F. A. *Nuclear Magnetic Resonance Spectroscopy*; Academic: New York, NY, 1969; pp 64–71.